# Anhydrite Dissolution Dynamics as a Hydrogeochemical Tracer of Seismic-Fluid Coupling: Insights from the East Anatolian Fault Zone, Turkey~~Gypsum as a potential tracer of earthquake: a case study of the *Mw*7.8 earthquake in the East Anatolian Fault Zone, southeastern Turkey~~

Zebin Luo[1], Xiaocheng Zhou[2,3], Yueren Xu[2], Peng Liang[2], Huiping Zhang[4], Jinlong Liang[5], Zhaojun Zeng[2], Yucong Yan[3], Zheng Gong[6], Shiguang Wang[6], Chuanyou Li[4], Zhikun Ren[4], Jingxing Yu[4], Zifa Ma[4], Junjie Li[4]

[1]School of Emergency Management, Xihua University, Chengdu 610039, China
[2]United Laboratory of High-Pressure Physics and Earthquake Science, institute of earthquake forecasting, CEA, Beijing 100036, China
[3]School of Earth Sciences and Resources, China University of Geosciences, Beijing 100083, China
[4]Institute of Geology, China Earthquake Administration, Beijing, 100081, China
[5]College of Earth and Planetary Sciences, Chengdu University of Technology, Chengdu 610059, China
[6] Institute of Geophysics, China Earthquake Administration, Beijing, 100081, China

*Correspondence to*: Xiaocheng Zhou (zhouxiaocheng188@163.com).

**Abstract:** Pre-seismic turbidity and salinity anomalies in groundwater were documented at HS04 and HS14 monitoring wells along the East Anatolian Fault Zone (EAFZ) following the 2023 *Mw* 7.8 and *Mw* 7.6 Turkey earthquakes. By synthesizing hydrogeochemical datasets (2013-20~~5~~3) with post-seismic responses, we unravel fault-segmented groundwater evolution: (1) Northern Na-Cl and Na-$HCO_3$ type waters result from mixing of mantle-derived magmatic fluids (0-7% contribution) with shallow groundwater, governed by volcanic rocks-carbonate dissolution; (2) Central-southern Ca-$HCO_3$ and Ca-Na-$HCO_3$ systems reflect shallow circulation with localized inputs from evaporites (Increased $SO_4^{2-}$ concentration caused by dissolution of anhydrite), ophiolites ($Mg^{2+}$ anomalies), and seawater. PHREEQC simulation shows that the dissolve-precipitation equilibrium of anhydrite is sensitive to the variation of water-rock reaction intensity in the Central-southern segments of EAFZ. Coseismic permeability changes disrupt the solubility equilibria of anhydrite, driving hydrochemical anomalies. We propose that seismic stress redistribution induces fracture network reorganization, thereby disrupting anhydrite solubility equilibria. Given its tectonic sensitivity and widespread occurrence, anhydrite dissolution dynamics emerge as a potential tracer for hydrogeochemical monitoring in active fault zones.

**Key words:** Groundwater; Water-rock interaction; Seismic activity; PHREEQC; Anhydrite; East Anatolian Fault Zone.Zebin Luo[1], Xiaocheng Zhou[2,3★], Yueren Xu[2], Peng Liang[2], Huiping Zhang[4], Jinlong Liang[5], Zhaojun Zeng[2], Yucong Yan[3], Zheng Gong[6], Shiguang Wang[6], Chuanyou Li[4], Zhikun Ren[4], Jingxing Yu[4], Zifa Ma[4], Junjie Li[4]

**1School of Emergency Management, Xihua University, Chengdu 610039, China**

**2United Laboratory of High-Pressure Physics and Earthquake Science, institute of earthquake forecasting, CEA, Beijing 100036, China**

**3School of Earth Sciences and Resources, China University of Geosciences, Beijing 100083, China**

**4Institute of Geology, China Earthquake Administration, Beijing, 100081, China**

**5College of Earth and Planetary Sciences, Chengdu University of Technology, Chengdu 610059, China**

**6 Institute of Geophysics, China Earthquake Administration, Beijing, 100081, China**

*** Corresponding author: Xiaocheng Zhou (zhouxiaocheng188@163.com).**

Key point:

**1. EAFZ geothermal fluid is obviously modified by earthquake, including: energy and materials.**

**2. EAFZ geothermal fluid is heavily diluted by the infiltration of a large amount of shallow cold water.**

**3. Shallow sedimentary minerals (e.g., gypsum) could be used as precursory anomaly indicators of earthquakes .**

★ Corresponding author

E-mail Address: *Xiaocheng Zhou (zhouxiaocheng188@163.com)*

**Abstract:**

**Obvious macroscopic anomalies of geothermal fluids were observed before and after the Mw 7.8 earthquake in Turkey. In order to find out the relationship between geothermal fluid anomalies and earthquakes, we performed a systematic hydrogeochemistry and isotopic analysis of the geothermal fluids in the East Anatolian Fault Zone (EAFZ). The results show that these geothermal fluids were reconstructed (including: energy and materials) by earthquakes. Based on chlorine – enthalpy model, the temperature of the deep geothermal fluid has been increasing to 382 $^{o}C$ on the strength of the energy released by the seismic activity. However, the information of the deep geothermal fluid was eventually covered due to the infiltration of a large amount of shallow cold water after the earthquake. The abnormal concentrations of $Ca^{2+}$ (54.04~501.58mg/L), $Mg^{2+}$ (6.58~116.20mg/L), $SO_4^{2-}$ (6.37~287.74mg/L), Sr (34.78~3244.8μg/L), and Ba (1.89~196.48μg/L) in geothermal water shown that the geothermal water has undergone complex water-rock interaction processes such as gypsum, calcite, dolomite, anorthite and serpentinization. Specially, significant gypsum dissolution was observed at HS05, HS09 and HS14 before and after the earthquake, suggesting that the earthquake broke the balance of water-rock reaction and promoted the dissolution of gypsum. Combined with geological background and previous studies, we propose that shallow sedimentary minerals, such as gypsum, have the potential to be used as earthquake warning indicators. However, shallow minerals are controlled by many external factors (e.g., temperature, pressure, climatic conditions, seasonal changes etc.), which greatly weakens their practical value in earthquake early warning.**

**Key words: Geothermal fluid; Water-rock interaction; Earthquake forecasting; PHREEQC; Gypsum; East Anatolian Fault Zone.**

## 1 Introduction

Active fault zones perturb subsurface hydrogeochemical equilibrium through dynamic rock-water interactions, generating diagnostic anomalies in groundwater chemistry that may serve as potential seismic precursors (Franchini et al., 2021; Ingebritsen and Manga, 2014; King et al., 2006; Luo et al., 2023; Poitrasson et al., 1999; Skelton et al., 2014; Tsunogai and Wakita, 1995; Wang et al., 2021). However, the diagnostic reliability of such hydrochemical signatures faces challenges. Climatic factors (e.g., precipitation variability and temperature fluctuations) can mask tectonic signals by altering water-rock reaction kinetics (Okan et al., 2018), while regional heterogeneity in lithology, fracture density, and hydrological circulation depth introduces substantial spatial variability in groundwater (Luo et al., 2023). This study investigates the hydrogeochemical characteristics of the seismically active East Anatolian Fault Zone (EAFZ) in eastern Turkey through a comprehensive 13-year observational dataset (2013–202~~5~~3). By systematically analyzing groundwater circulation patterns and water-rock interaction processes along the fault system, we integrate post-seismic hydrochemical monitoring following the February 2023 *Mw* 7.8 and 7.6 earthquake sequence to delineate the relationship between hydrogeochemical anomalies and fault activity. Our findings aim to establish the relationship between groundwater anomalies and fault zone activities, thereby advancing methodologies for groundwater-based seismic monitoring in active fault zone systems.

The EAFZ, a ~500 km NE-SW trending left-lateral strike-slip system accommodating ~11 mm/yr of Anatolian-Arabian plate motion with reverse thrust components (Pousse‐Beltran et al., 2020), has generated destructive seismic events throughout recorded history (Hubert-Ferrari et al., 2020; Simão et al., 2016; Sparacino et al., 2022; Tan et al., 2008). The 2023 twin earthquakes exemplify its capacity for massive stress release (Kwiatek et al., 2023; Ma et al., 2024; Wang et al., 2023b), producing coseismic surface ruptures exceeding 280 km with maximum slip of 7.2±0.72 m (Liang et al., 2024). Notably, marked hydrochemical anomalies (e.g., white water, turbidity and intermittent groundwater gushing) were detected at monitoring wells HS04 and HS14 both before and after the earthquake (Video 1 and 2), indicating fault-controlled fluid responses to seismic stress perturbations.

Previous studies have identified three primary fluid sources within the EAFZ system: 1) mantle-derived magmatic fluids (Aydin et al., 2020; Italiano et al., 2013; Karaoğlu et al., 2019), 2) deeply circulated metamorphic waters (Yuce et al., 2014), and 3) Mediterranean seawater intrusion at its southern terminus

(Yuce et al., 2014). These studies provide sufficient data support for accurate understanding of EAFZ groundwater circulation. In this contribution, the EAFZ groundwater observation data over the past 13 years are compared with the groundwater chemical composition after the double earthquakes in 2023 to tracing the origin of geothermal fluid, restore the water-rock interaction process, and evaluate the influence of seismic activity on the geothermal fluid circulation process. This work provides new constraints on tectonic controls of deep fluid migration in active fault zone systems while advancing the application of hydrogeochemical monitoring in seismic hazard assessment.

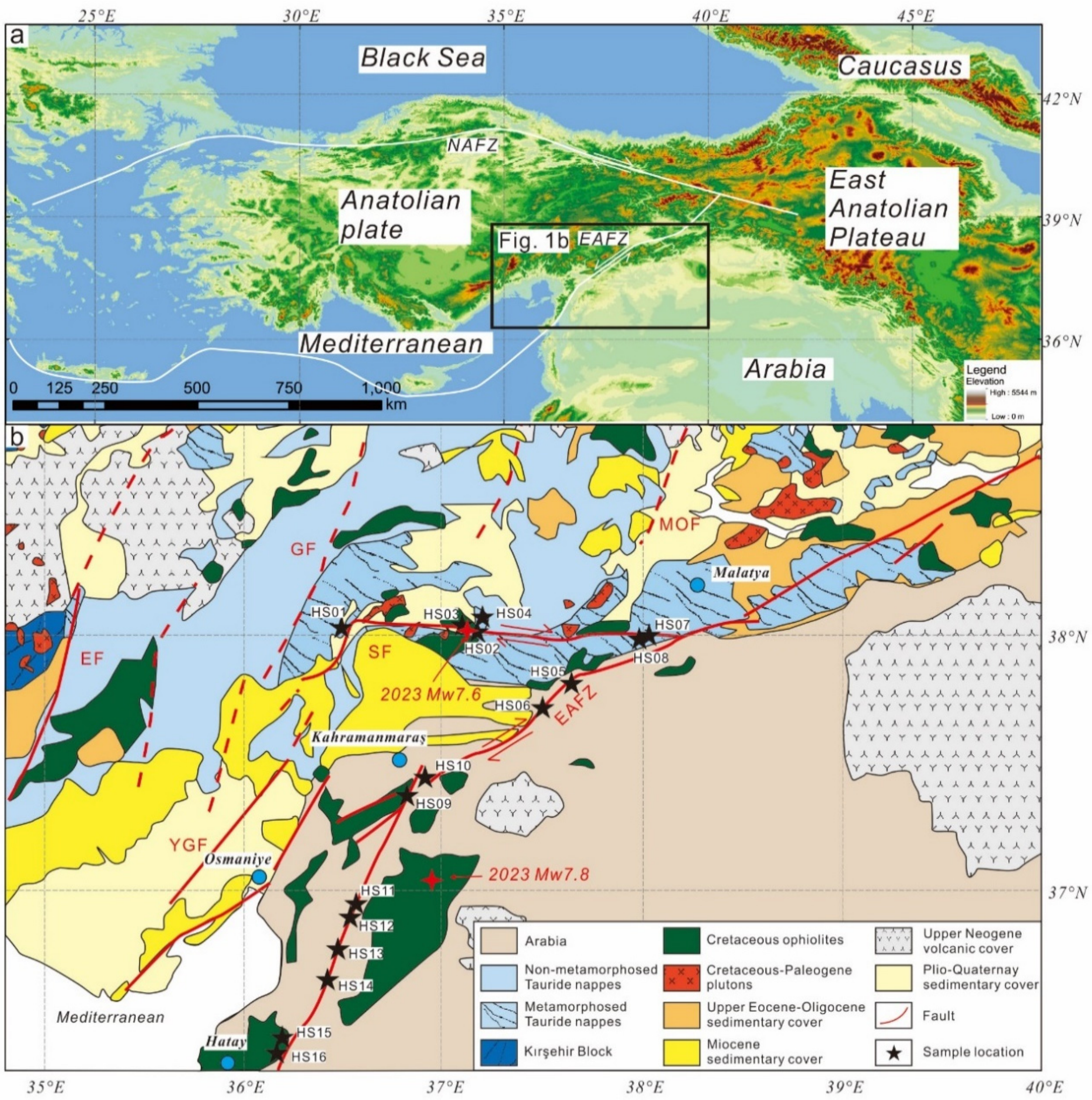


**Fig. 1. a: A brief Map of the eastern Mediterranean region from NASADEM (https://doi.org/10.5069/G93T9FD9). b: Geological map of EAFZ, modified from (van Hinsbergen et al., 2024). EF: Ecemiş Fault, SF: Sürgü Fault, MOF: Malatya-Ovacık Fault, GF: Göksün Fault, YGF: Yeşilgöz-Göksün Fault.**

~~On February 6, 2023, southeastern Turkey were struck by a series of devastating earthquakes. The two main earthquakes were Mw 7.8 and Mw 7.6, followed by multiple aftershocks (Including one of Mw 6.7 and several earthquakes of greater than Mw 4) (Kwiatek et al., 2023; Ni et al., 2023). The main areas affected by these earthquakes include the provinces of Qahraman, Marash and Hatay. According to official statistics, more than 60,000 people have been killed and millions displaced in southern Turkey and northern Syria (Ma et al., 2024; Över et al., 2023; Wang et al., 2023b).~~

~~The double earthquakes in February 2023 occurred along the East Anatolian Fault Zone (EAFZ), one of the more seismically active seismic zones in the world (Whitney et al., 2023). There have been many ruinous earthquakes in history (Hubert-Ferrari et al., 2020; Simão et al., 2016; Sparacino et al., 2022; Tan et al., 2008). Research shows that, at present, East Anatolian fault zone has a left-lateral strike-slip rate of ~11 mm/yr (Pousse‐Beltran et al., 2020). Meanwhile, it is accompanied by a certain thrust process, which causes huge stresses at the plate margin. The massive stress release is the main cause of the February 2023 earthquakes (Kwiatek et al., 2023; Ma et al., 2024; Wang et al., 2023b). Before and after earthquakes, obvious macroscopic anomalies were observed in many hot springs (HS04 and HS14) (Fig. S1), which indicates the fact that the geothermal fluid circulation has been disturbed by seismic activity.~~

~~As the important medium of seismic monitoring research, geothermal fluids are widely used in the world e.g., (Franchini et al., 2021; King et al., 2006; Luo et al., 2023; Poitrasson et al., 1999; Skelton et al., 2014; Tsunogai and Wakita, 1995; Wang et al., 2021). Many important theoretical achievements have been made in the direction of earthquake monitoring and early warning. For example: Changes in groundwater chemistry before two consecutive earthquakes in Iceland (Skelton et al., 2014), Precursory Chemical Changes in Ground Water: Kobe Earthquake, Japan (Tsunogai and Wakita, 1995), etc. However, there is a serious problem that the geothermal fluid anomaly index is not universal. In other words, it is difficult to promote and apply in the world (Luo et al., 2023). The fundamental reason is the complexity of geothermal fluid cycle. Exactly, the two earthquakes in February 2023 in Turkey provides an opportunity to explore the relationship between geothermal fluids and earthquakes. Therefore, the geothermal fluids in the EAFZ are systematically studied in this contribution to tracing the origin of geothermal fluid, restore the water-rock interaction process, and evaluate the influence of seismic activity on the geothermal fluid circulation process. This study would help to deepen the understanding of the influence of earthquakes on geothermal fluid, and provide data reference for earthquake monitoring and early warning research.~~

## 2 Geologic background

Located at the intersection of Eurasia, Africa and Arabia, Turkey has a complex tectonic background~~Located at the intersection of Eurasia, Africa and Arabia, Turkey is a complex tectonic collage~~ (Lanari et al., 2023; Simão et al., 2016). Here, the collision between the Arabian and Eurasian plates was an important tectonic process that began in the early Miocene (~ 23 Ma) and continues to the this day (van Hinsbergen et al., 2024). This collision caused plateau uplift, volcanic eruptions, sedimentary basin formation, and large-scale strike-slip faults in eastern Turkey, including the EAFZ (Fig. 1) (Bilim et al., 2018; Karaoğlu et al., 2018; Karaoğlu et al., 2020; Whitney et al., 2023; Yönlü et al., 2017; Zhou et al., 2024).

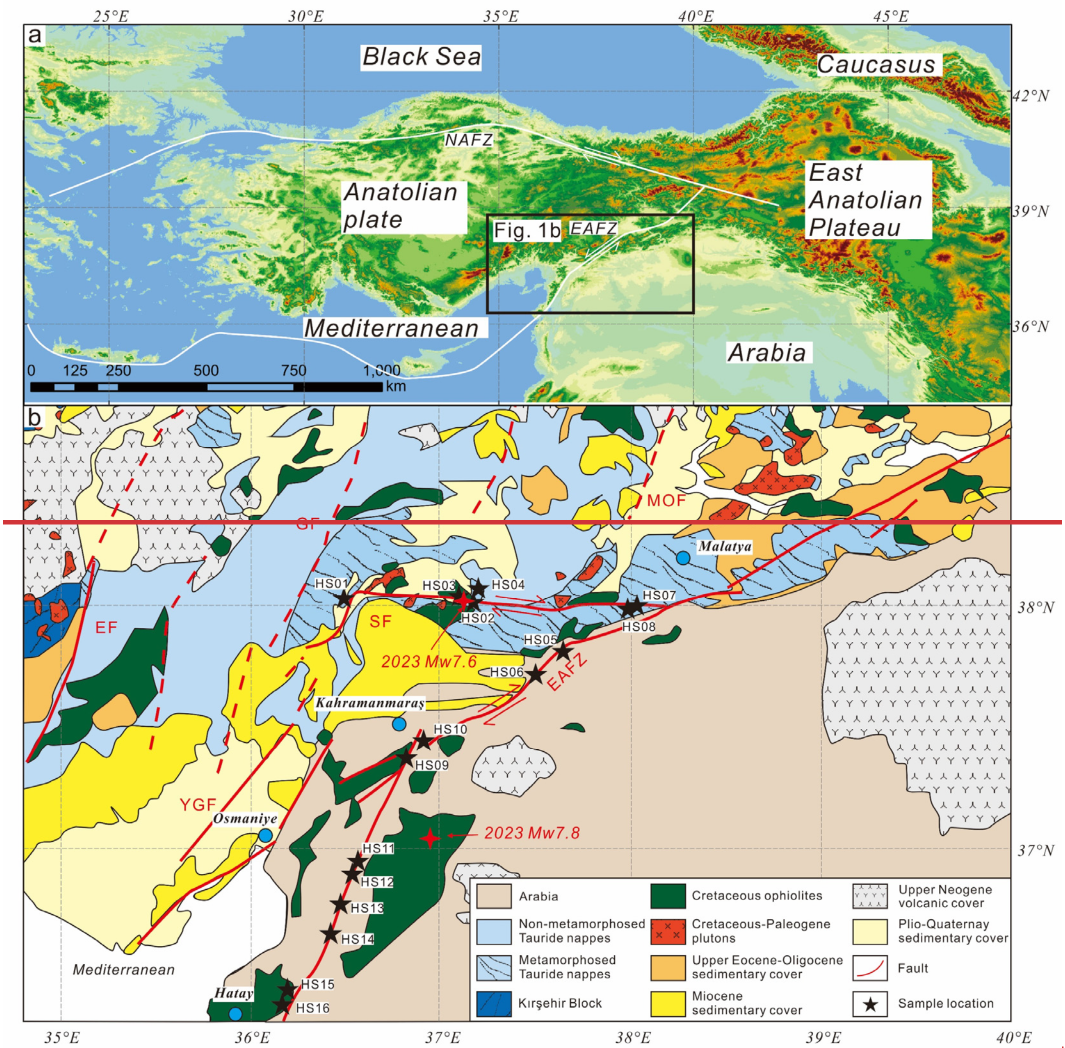


~~Figure 1. a: A brief Map of the eastern Mediterranean region from Google earth. b: Geological map of EAFZ, modified from (van Hinsbergen et al., 2024). EF: Ecemiş Fault, SF: Sürgü Fault, MOF: Malatya-Ovacık Fault, GF: Göksün Fault, YGF: Yeşilgöz-Göksün Fault.~~

The formation of the EAFZ is related to the northward subduction of a strong and thin lithospheric wedge under the Arabian Plate (Nalbant et al., 2002; Sparacino et al., 2022). This subduction process led to the formation of a stress concentration zone that eventually developed into a strike-slip fault that penetrated the entire lithosphere, i.e. the EAFZ (Nalbant et al., 2002). In addition, because the African plate and the

Arabian plate are still moving northward, this fault zone is also accompanied by a certain thrust process, which causes huge stresses at the plate margin (Ma et al., 2024; Över et al., 2023; Özkan et al., 2023; Pousse‐Beltran et al., 2020; Wang et al., 2023b; Whitney et al., 2023).

The stratigraphic composition of the East Anatolian fault zone is complex, including Non-metamorphosed Tauride nappes and Metamorphosed Tauride nappes crystallization base, Cretaceous ophiolites and Cretaceous-Paleogene plutons. It is overlaid by clastic deposits, lacustrine deposits (such as: Ancient Amik Lake) and volcanic cover of Upper Eocene-Oligocene to Plio-Quaternay. Faults are widely developed in study area, including East Anatolian Fault, Ecemiş Fault, Sürgü Fault, Malatya-Ovacık Fault, Göksün Fault, Yeşilgöz-Göksün Fault etc. (van Hinsbergen et al., 2024). These faults has been active for a long time and has a history of devastating earthquakes, including two in February 2023 (*Mw* 7.8 and *Mw* 7.6) (Fig. 1) (Carena et al., 2023; Kwiatek et al., 2023; Ma et al., 2024; Maden and Öztürk, 2015; Över et al., 2023; Özkan et al., 2023; Pousse‐Beltran et al., 2020; Tan et al., 2008; Wang et al., 2023b).

The climate of the EAFZ is mainly a temperate continental climate with cold winters and hot and dry summers. The average annual rainfall is between 200 mm and 600 mm, and is mainly winter rain. Due to its inland location and low rainfall, the flow of the river is relatively small. The groundwater system is relatively complex, and geothermal resources are mainly distributed near the fault zone and its controlled areas, including low or moderate temperature geothermal systems, which have great potential for development and utilization (Aydin et al., 2020; Güleç and Hilton, 2016; Inguaggiato et al., 2016; Karaoğlu et al., 2019).

## 3 Sampling and analytical methods

16 samples of groundwater~~water~~ were collected in EAFZ, including hot springs, geothermal wells and river water. HS01-HS04 was collected from west to east along SF. HS07-HS16 was collected from north to south along EAFZ (Fig. 1). Detailed sample collection and testing methods can be found at Luo et al. (2023). In short, the water sample was taken with a 50 mL clean polyethylene bottle and the temperature and pH of the water were measured and recorded. Two samples were~~are~~ collected at each sampling site, one ~~is~~ was added with ultrapure $HNO_3$ to analyse the cation content, and the other ~~is~~ was used to analyse

the anion content and isotopic composition. All samples need to be pre-treated with a 0.45 μm filter membrane to remove impurities before samplingbefore being tested. The Hydrogen and oxygen isotopes were determined by a Picarro L2140-I Liquid water and vapor isotope analyzer (relative to Vienna Standard Mean Ocean Water (V - SMOW)). Precisions on the measured $\delta^{18}O$ and $\delta D$ value was ±0.2% (2SD) and ±1% (2SD) respectively (Zeng et al., 2025). The cation ($Li^{+}$, $Na^{+}$, $K^{+}$, $Ca^{2+}$and $Mg^{2+}$) and anion ($F^{-}$, $Cl^{-}$, $NO_3^{-}$ and $SO_4^{2-}$) were analysed by Dionex ICS-900 ion chromatograph (Thermo Fisher Scientific Inc.) at the Earthquake Forecasting Key Laboratory of China Earthquake Administration, with the reproducibility within ±2% and detection limits 0.01 mg/L (Chen et al., 2015). $HCO_3^{-}$ and $CO_3^{2-}$ was determined by acid-base titration with a ZDJ-100 potentiometric titrator (reproducibility within ±2%). $SiO_2$ were analysed by inductively coupled plasma emission spectrometer Optima-5300 DV (PerkinElmer Inc.) (Li et al. 2021). Trace elements were analysed by Element XR ICP-MS at the Test Center of the Research Institute of Uranium Geology. Multielement standard solutions (IV-ICPMS 71A, IV-ICP-MS 71B and IV-ICP-MS 71D, iNORGANIC VENTURES) used for quality control. The analytical error margin of major cations and trace elements were less than 10%. Strontium isotope ratios ($^{87}Sr/^{86}Sr$) were determined through triple quadrupole ICP-MS (Agilent 8900 ICP-QQQ) with a precision of ±0.001 (Liu et al., 2020).MAT 253 was used to analyses $\delta D$ and $\delta^{18}O$ (relative to Vienna Standard Mean Ocean Water (V - SMOW)). The cation and anion were analysed by Dionex ICS-900 ion chromatograph (Thermo Fisher Scientific Inc.). $HCO_3^{-}$ and $CO_3^{2-}$ was determined by acid-base titration with a ZDJ-100 potentiometric titrator. $SiO_2$ were analysed by inductively coupled plasma emission spectrometer Optima-5300 DV (PerkinElmer Inc.). Trace elements were analysed by Element XR ICP-MS. Multielement standard solutions (IV-ICPMS 71A, IV-ICP-MS 71B and IV-ICP-MS 71D, iNORGANIC VENTURES) used for quality control (the analytical error margin of major cations and trace elements were less than 10%).

## 4 Results

Physical, chemical and isotopic compositions of groundwatersgeothermal water are listed in Table 1. The pH of the water samples varied from 7.03 to 11.72, and all the samples showed weakly alkaline characteristics except HS15 (pH=11.72). The effluent temperature of water sample is low (8.1~32.0~~32~~°C), and the highest temperature is HS15 well sample (32.0°C). HS08 is a river sample with the lowest temperature (8.1°C). $SiO_2$ varies from 0.38 mg/L to 84.64mg/L~~, and the closer to the epicenter, the higher the $SiO_2$ content.~~. $HCO_3^-$ (165.72~1854.30 mg/L) is the main anion. The concentration of $SO_4^{2-}$ range from 1.21 mg/L to 316.61 mg/L, and the concentration of $SO_4^{2-}$ in some samples is relatively high (e.g. HS01 (287.74 mg/L), HS03 (103.56 mg/L), HS04 (229.75 mg/L), HS14 (316.61 mg/L))~~The concentration of $SO_4^{2-}$ range from 1.21 mg/L to 316.61 mg/L, and the concentration of $SO_4^{2-}$ in some samples is obviously increased (e.g. HS01, HS03, HS04, HS14)~~. The concentration of $Na^+$ (0.42~88.93 mg/L), $Cl^-$ (0.97~75.92 mg/L) and B (3.62~1047.25 μg/L) varied synergistically~~changed synergistically~~. The $Na^+$, $Cl^-$ and B content of HS14, HS15 and HS16 increased significantly. $Ca^{2+}$ (14.16~501.58 mg/L) is the main cation, followed by $Mg^{2+}$ (0.38~116.2 mg/L). The types of geothermal water include Na-Cl-$HCO_3$, Ca-$HCO_3$, Ca-$HCO_3$-$SO_4$ and Mg-$HCO_3$ (Fig. 2). The $\delta^{18}O$ and δD of samples varied from –11.30‰ to –6.55‰ and –65.43‰ to –34.43‰ respectively, which is near to the global meteoric water line (GMWL) (Craig, 1961) (Fig. 3), suggesting their meteoric water origin. The $^{87}Sr/^{86}Sr$ varied from 0.7053 to 0.7135, showing the characteristics of multi-source region mixing.

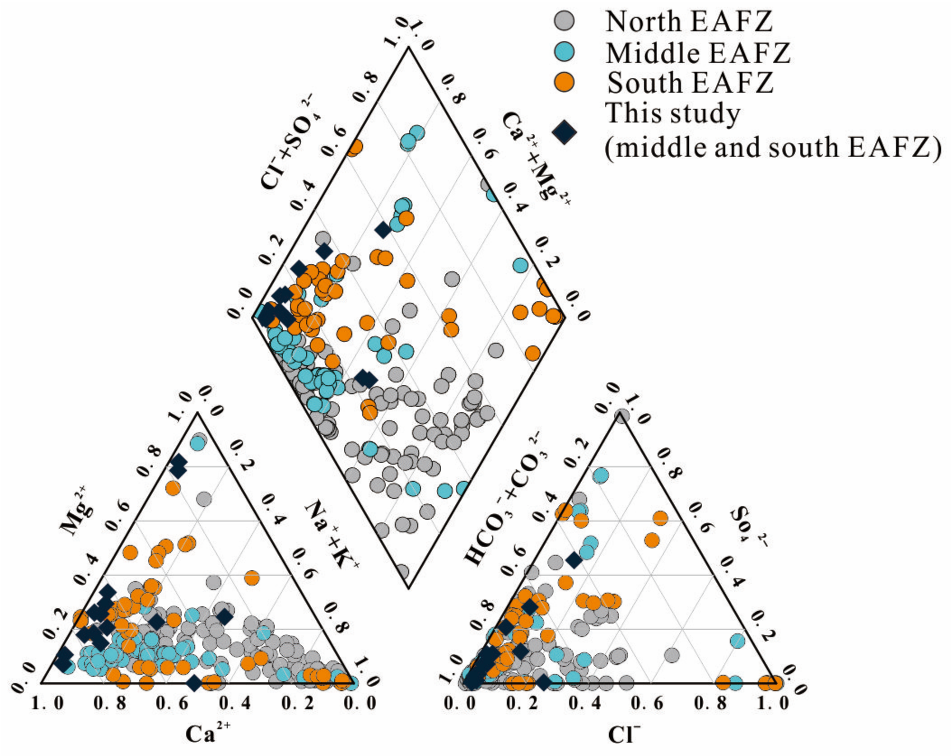


**Fig. 2. Piper plot of sampled groundwaters in EAFZ. The groundwaters are Na-Cl-$HCO_3$, Ca-$HCO_3$, Ca-$HCO_3$-$SO_4$ and Mg-$HCO_3$ types. Literature data source (see Table S1 for details): (Aydin et al., 2020; Baba et al., 2019; Karaoğlu et al., 2019; Okan et al., 2018; Pasvanoglu, 2020; YASİN and YÜCE, 2023; Yuce et al.,**

2014)

The composition of trace elements in geothermal fluids are shown in Table 2. The contents of Sr (30.13~3244.88 μg/L) and Ba (1.89~196.48 μg/L) in the samples varied widely. Moreover, Sr and $SO_4^{2-}$ had obvious positive correlation. Box plot analysis showed that the Fluid-Mobile Element (FME) concentrations of B (3.62–1047.25 μg/L), Li (0.33–89.93 μg/L) and Rb (0.14–28.91 μg/L) in some samples were greater than the median (Fig. S1).~~Statistical analysis shows that the concentration of fluid activity elements, such as B (3.62~1047.25 μg/L), Li (0.33~89.93 μg/L) and Rb (0.14~28.91 μg/L), are at historic highs versus (Fig. S2).~~ Enrichment coefficients (EF) normalized by Ti is used for geothermal fluids and rocks. The result shows that Whether compared with schist, basalt or Andesite of EAFZ, trace elements in geothermal fluids are all in a state of enrichment, and some elements can even be enriched 100000 times (Fig. S3).

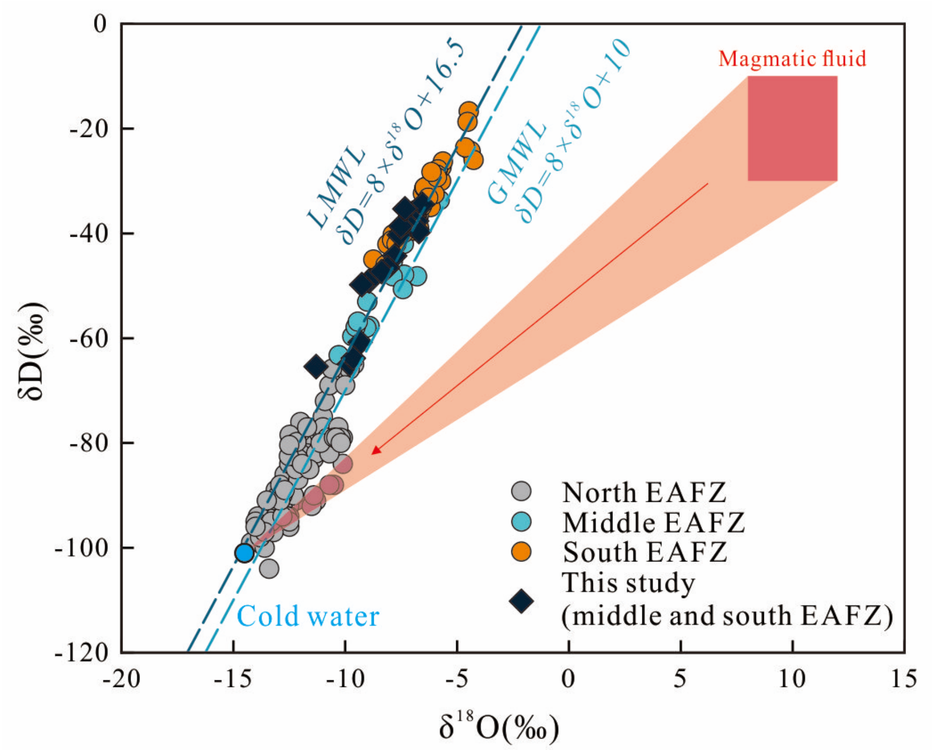


**Fig. 3. δD and $\delta^{18}O$ (‰V-SMOW) values for groundwaters collected from EAFZ. The GMWL represents the global meteoric water line (Craig, 1961). The LMWL represents the Local meteoric water line (Aydin et al., 2020). The magmatic fluid distribution (δD = −20 ± 10‰, $\delta^{18}O$ = 10 ± 2‰) from (Giggenbach, 1992). Literature data source is consistent with Fig. 2.**

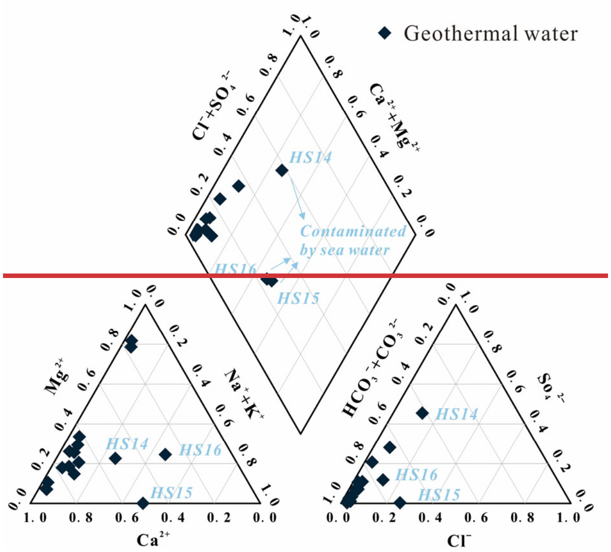


Figure 2. Piper plot of sampled geothermal waters in EAFZ. The geothermal waters are Na-Cl-HCO$_3$, Ca-HCO$_3$, Ca-HCO$_3$-SO$_4$ and Mg-HCO$_3$ types.

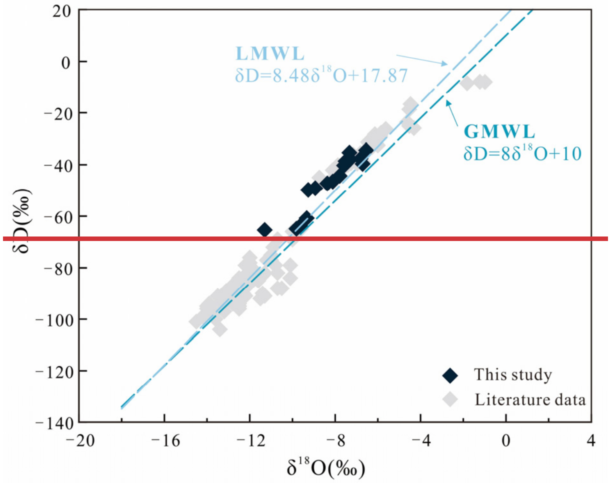


Figure 3. δD and δ$^{18}$O (‰V-SMOW) values for geothermal waters collected from EAFZ. The GMWL represents the global meteoric water line (Craig, 1961). According to this study and literature data (Aydin et al., 2020; Yuce et al., 2014), Local Meteoric Water Line (LMWL) is δD = 8.48 δ$^{18}$O+17.87 ($R^2$=0.95, n=110).

Table 1.Physical, Chemistry and isotopic compositions of groundwaters from the EAFZ.

| No | Long (E) (°) | lat (N) (°) | Type | Date | T (°C) | pH | EC (μS/cm) | $SiO_2$ (mg/L) | $Li^+$ (mg/L) | $Na^+$ (mg/L) | $K^+$ (mg/L) | $Mg^{2+}$ (mg/L) | $Ca^{2+}$ (mg/L) | $F^-$ (mg/L) | $Cl^-$ (mg/L) | $NO_3^-$ (mg/L) | $SO_4^{2-}$ (mg/L) | $HCO_3^-$ (mg/L) | $CO3^{2-}$ (mg/L) | δD (‰) | $\delta^{18}O$ (‰) | $^{87}Sr/^{86}Sr$ | 2SD |
|---|---|---|---|---|---|---|---|---|---|---|---|---|---|---|---|---|---|---|---|---|---|---|---|
| HS01 | *36.518113* | *38.003517* | S | 03/23/2024 | 15.8 | 8.12 | 1565 | 20.70 | - | 27.93 | 4.85 | 75.69 | 253.85 | 3.60 | 55.46 | - | 287.74 | 670.01 | - | - | -9.81 | 0.7065 | 0.0001 |
| HS02 | *37.173212* | *38.028567* | S | 03/23/2024 | 13.2 | 8.35 | 287 | 5.27 | - | 0.42 | - | 6.58 | 54.04 | 0.40 | 1.33 | 5.06 | 6.37 | 178.53 | - | - | - | 0.7120 | 0.0003 |
| HS03 | *37.166040* | *38.031327* | S | 03/23/2024 | 13.2 | 7.12 | 1876 | 26.36 | 0.13 | 48.44 | 0.48 | 74.20 | 368.42 | 0.50 | 30.85 | 30.13 | 103.56 | 1271.1 | - | - | -9.33 | 0.7079 | 0.0002 |
| HS04 | *37.174886* | *38.033718* | S | 03/23/2024 | 15.0 | 7.03 | 2683 | 84.64 | 0.05 | 19.90 | 0.46 | 116.20 | 501.58 | 3.70 | 9.29 | 3.33 | 229.75 | 1854.3 | - | - | -9.64 | 0.7132 | 0.0008 |
| HS05 | *37.669088* | *37.809271* | S | 03/23/2024 | 12.7 | 8.50 | 634 | 14.42 | - | 7.66 | 0.39 | 25.88 | 103.61 | 0.53 | 4.43 | 12.92 | 29.75 | 367.72 | - | - | -7.79 | 0.7091 | 0.0003 |
| HS06 | *37.510811* | *37.700516* | S | 03/23/2024 | 15.0 | 8.27 | 774 | 15.34 | - | 4.19 | 0.32 | 54.08 | 100.99 | 0.43 | 5.98 | 1.61 | 7.96 | 515.66 | - | - | -8.11 | 0.7100 | 0.0002 |
| HS07 | *38.056844* | *37.942560* | S | 03/23/2024 | 9.8 | 8.46 | 276 | 9.41 | - | 0.84 | - | 4.62 | 55.11 | 0.41 | 0.97 | 2.74 | 5.00 | 167.86 | - | - | -8.93 | 0.7135 | 0.0006 |
| HS08 | *38.051818* | *37.939222* | R | 03/23/2024 | 8.1 | 8.43 | 275 | 15.15 | - | 1.13 | - | 4.47 | 55.34 | 0.44 | 1.06 | 3.83 | 5.69 | 165.72 | - | - | -9.26 | 0.7104 | 0.0004 |
| HS09 | *36.808379* | *37.349742* | S | 03/23/2024 | 18.0 | 8.11 | 699 | 25.50 | 0.01 | 5.85 | 0.21 | 42.60 | 94.99 | 0.52 | 6.80 | 8.87 | 93.44 | 344.96 | - | - | -6.81 | 0.7076 | 0.0002 |
| HS10 | *36.994384* | *37.460028* | S | 03/23/2024 | 20.0 | 8.48 | 659 | 31.29 | - | 1.57 | - | 90.13 | 18.22 | 0.35 | 3.80 | 7.53 | 2.76 | 459.47 | - | - | -6.71 | 0.7119 | 0.0003 |
| HS11 | *36.554302* | *36.892454* | S | 03/23/2024 | 16.3 | 8.27 | 517 | 9.69 | - | 2.32 | 0.09 | 27.89 | 75.25 | 0.45 | 4.39 | 9.25 | 12.11 | 312.24 | - | - | -7.58 | 0.7107 | 0.0004 |
| HS12 | *36.521328* | *36.811041* | S | 03/23/2024 | 16.9 | 8.32 | 489 | 46.50 | - | 2.11 | - | 60.76 | 14.16 | 0.52 | 6.13 | 14.55 | 4.27 | 307.98 | - | - | -6.55 | 0.7110 | 0.0006 |
| HS13 | *36.439440* | *36.672020* | S | 03/23/2024 | 18.2 | 8.22 | 579 | 10.05 | 0.01 | 4.87 | 0.49 | 30.35 | 81.56 | 0.50 | 7.67 | 8.67 | 39.89 | 309.40 | - | - | -7.30 | 0.7080 | 0.0002 |
| HS14 | *36.373823* | *36.503634* | W | 03/23/2024 | 23.5 | 8.21 | 1305 | 36.64 | 0.09 | 62.40 | 5.79 | 65.12 | 151.43 | 4.33 | 75.92 | 34.60 | 316.61 | 300.15 | - | - | -7.51 | 0.7053 | 0.0001 |
| HS15 | *36.163672* | *36.383335* | S | 03/23/2024 | 32.0 | 11.72 | 589 | 0.38 | 0.02 | 48.64 | 1.42 | 0.38 | 55.55 | 0.41 | 48.71 | 5.28 | 1.21 | - | 154.61 | - | -8.37 | 0.7070 | 0.0007 |
| HS16 | *36.147159* | *36.273720* | S | 03/23/2024 | 24.5 | 8.45 | 1100 | 32.57 | 0.01 | 88.93 | 18.68 | 59.60 | 73.35 | 0.72 | 67.11 | 43.51 | 75.90 | 484.37 | - | - | -7.33 | 0.7073 | 0.0002 |

Note: "-" represents below detection limit or undetected. "S" is Hot spring, "W" is Well water, "R" is river water.

Table 1.Physical, Chemistry and isotopic compositions of geothermal waters from the EAFZ.

| No | Long (E) | lat (N) | Type | Date | T | pH | EC | $SiO_2$ | $Li^+$ | $Na^+$ | $K^+$ | $Mg^{2+}$ | $Ca^{2+}$ | $F^-$ | $Cl^-$ | $NO_3^-$ | $SO_4^{2-}$ | $HCO_3^-$ | $CO3^{2-}$ | δD | $\delta^{18}O$ |
|---|---|---|---|---|---|---|---|---|---|---|---|---|---|---|---|---|---|---|---|---|---|
| | (° ) | (° ) | | | (°C) | | (μS/cm) | (mg/L) | (mg/L) | (mg/L) | (mg/L) | (mg/L) | (mg/L) | (mg/L) | (mg/L) | (mg/L) | (mg/L) | (mg/L) | (mg/L) | (‰) | (‰) |
| HS01 | *36.52* | *38.00* | S | 03/22/2024 | 15.8 | 8.12 | 1565 | 20.7 | - | 27.93 | 4.85 | 75.69 | 253.85 | 3.6 | 55.46 | - | 287.74 | 670.01 | - | -64.93 | -9.81 |
| HS02 | *37.17* | *38.03* | S | 03/22/2024 | 13.2 | 8.35 | 287 | 5.27 | - | 0.42 | - | 6.58 | 54.04 | 0.4 | 1.33 | 5.06 | 6.37 | 178.53 | - | -65.43 | -11.30 |
| HS03 | *37.17* | *38.03* | S | 03/22/2024 | 13.2 | 7.12 | 1876 | 26.36 | 0.13 | 48.44 | 0.48 | 74.2 | 368.42 | 0.5 | 30.85 | 30.13 | 103.56 | 1271.1 | - | -60.77 | -9.33 |
| HS04 | *37.17* | *38.03* | S | 03/22/2024 | 15 | 7.03 | 2683 | 84.64 | 0.05 | 19.9 | 0.46 | 116.2 | 501.58 | 3.7 | 9.29 | 3.33 | 229.75 | 1854.3 | - | -63.82 | -9.64 |
| HS05 | *37.67* | *37.81* | S | 03/23/2024 | 12.7 | 8.5 | 634 | 14.42 | - | 7.66 | 0.39 | 25.88 | 103.61 | 0.53 | 4.43 | 12.92 | 29.75 | 367.72 | - | -44.29 | -7.79 |
| HS06 | *37.51* | *37.70* | S | 03/23/2024 | 15 | 8.27 | 774 | 15.34 | - | 4.19 | 0.32 | 54.08 | 100.99 | 0.43 | 5.98 | 1.61 | 7.96 | 515.66 | - | -46.53 | -8.11 |
| HS07 | *38.06* | *37.94* | S | 03/23/2024 | 9.8 | 8.46 | 276 | 9.41 | - | 0.84 | - | 4.62 | 55.11 | 0.41 | 0.97 | 2.74 | 5 | 167.86 | - | -49.09 | -8.93 |
| HS08 | *38.05* | *37.94* | R | 03/24/2024 | 8.1 | 8.43 | 275 | 15.15 | - | 1.13 | - | 4.47 | 55.34 | 0.44 | 1.06 | 3.83 | 5.69 | 165.72 | - | -49.81 | -9.26 |
| HS09 | *36.81* | *37.35* | S | 03/24/2024 | 18 | 8.11 | 699 | 25.5 | 0.01 | 5.85 | 0.21 | 42.6 | 94.99 | 0.52 | 6.8 | 8.87 | 93.44 | 344.96 | - | -37.65 | -6.81 |
| HS10 | *36.99* | *37.46* | S | 03/25/2024 | 20 | 8.48 | 659 | 31.29 | - | 1.57 | - | 90.13 | 18.22 | 0.35 | 3.8 | 7.53 | 2.76 | 459.47 | - | -39.65 | -6.71 |
| HS11 | *36.55* | *36.89* | S | 03/25/2024 | 16.3 | 8.27 | 517 | 9.69 | - | 2.32 | 0.09 | 27.89 | 75.25 | 0.45 | 4.39 | 9.25 | 12.11 | 312.24 | - | -40.30 | -7.58 |
| HS12 | *36.52* | *36.81* | S | 03/25/2024 | 16.9 | 8.32 | 489 | 46.5 | - | 2.11 | - | 60.76 | 14.16 | 0.52 | 6.13 | 14.55 | 4.27 | 307.98 | - | -34.43 | -6.55 |
| HS13 | *36.44* | *36.67* | S | 03/26/2024 | 18.2 | 8.22 | 579 | 10.05 | 0.01 | 4.87 | 0.49 | 30.35 | 81.56 | 0.5 | 7.67 | 8.67 | 39.89 | 309.4 | - | -37.88 | -7.30 |
| HS14 | *36.37* | *36.50* | W | 03/26/2024 | 23.5 | 8.21 | 1305 | 36.64 | 0.09 | 62.4 | 5.79 | 65.12 | 151.43 | 4.33 | 75.92 | 34.6 | 316.61 | 300.15 | - | -38.61 | -7.51 |
| HS15 | *36.16* | *36.38* | S | 03/26/2024 | 32 | 11.72 | 589 | 0.38 | 0.02 | 48.64 | 1.42 | 0.38 | 55.55 | 0.41 | 48.71 | 5.28 | 1.21 | - | 154.61 | -47.27 | -8.37 |
| HS16 | *36.15* | *36.27* | S | 03/27/2024 | 24.5 | 8.45 | 1100 | 32.57 | 0.01 | 88.93 | 18.68 | 59.6 | 73.35 | 0.72 | 67.11 | 43.51 | 75.9 | 484.37 | - | -35.34 | -7.33 |

Note: “ ” represents below detection limit or undetected. “S” is Hot spring, “W” is Well water, “R” is river water.

Table 2.Trace elements compositions of groundwaters~~geothermal waters~~ from the EAFZ.

| No | B | Al | P | Sc | Ti | V | Mn | Fe | Co | Ni | Ga | Rb | Sr | Y | Zr | Nb | Ba | Hf | Ta | Pb | Th | U |
|---|---|---|---|---|---|---|---|---|---|---|---|---|---|---|---|---|---|---|---|---|---|---|
| | (μg/L) | (μg/L) | (μg/L) | (μg/L) | (μg/L) | (μg/L) | (μg/L) | (μg/L) | (μg/L) | (μg/L) | (μg/L) | (μg/L) | (μg/L) | (μg/L) | (μg/L) | (μg/L) | (μg/L) | (μg/L) | (μg/L) | (μg/L) | (μg/L) | (μg/L) |
| HS01 | 35.49 | 10.02 | 66.41 | 0.04 | 0.20 | 0.23 | 369.58 | 34.43 | 0.40 | 3.40 | 0.03 | 1.68 | 1231.40 | 0.04 | 0.19 | 0.02 | 77.45 | 0.004 | 0.01 | 0.19 | 0.001 | 3.15 |
| HS02 | 3.62 | 8.26 | 8.94 | 0.02 | 0.22 | 0.85 | 0.73 | 21.10 | 0.01 | 0.16 | 0.04 | 0.25 | 99.69 | 0.01 | - | 0.02 | 16.12 | - | 0.01 | 0.14 | - | 0.43 |
| HS03 | 1047.25 | 8.23 | 11.86 | 0.08 | 0.19 | 0.56 | 0.80 | 23.29 | 0.03 | 4.22 | 0.04 | 5.95 | 691.57 | 0.01 | 0.01 | 0.01 | 5.52 | 0.001 | 0.01 | 0.10 | - | 1.32 |
| HS04 | 512.31 | 6.75 | 12.88 | 0.58 | 0.22 | 0.19 | 890.21 | 563.31 | 4.06 | 19.67 | 0.01 | 28.91 | 1505.17 | 0.12 | 0.66 | 0.02 | 11.28 | 0.004 | 0.01 | 0.13 | 0.003 | 0.23 |
| HS05 | 43.88 | 6.88 | 9.14 | 0.04 | 0.17 | 2.23 | 0.90 | 16.14 | 0.04 | 0.88 | 0.04 | 0.31 | 667.55 | 0.02 | 0.03 | 0.01 | 196.48 | 0.001 | 0.01 | 0.17 | - | 1.64 |
| HS06 | 18.60 | 4.50 | 8.79 | 0.03 | 0.18 | 2.74 | 0.67 | 13.54 | 0.02 | 6.23 | 0.01 | 0.37 | 213.59 | 0.02 | 0.03 | 0.01 | 38.11 | 0.001 | 0.01 | 0.15 | - | 0.51 |
| HS07 | 8.32 | 12.99 | 10.51 | 0.01 | 0.20 | 2.09 | 3.58 | 81.59 | 0.02 | 0.37 | 0.11 | 0.49 | 53.27 | 0.03 | 0.01 | 0.01 | 3.48 | - | 0.01 | 0.26 | 0.004 | 0.32 |
| HS08 | 4.77 | 12.27 | 8.89 | 0.03 | 0.18 | 2.85 | 1.05 | 12.52 | 0.02 | 0.26 | 0.01 | 0.44 | 55.78 | 0.06 | - | 0.01 | 1.89 | - | - | 0.10 | - | 0.26 |
| HS09 | 24.05 | 8.48 | 4.56 | 0.04 | 0.27 | 0.50 | 0.99 | 45.62 | 0.01 | 0.81 | 0.02 | 0.62 | 967.07 | 0.02 | - | 0.01 | 105.53 | - | - | 0.15 | - | 0.49 |
| HS10 | 14.56 | 8.37 | 9.74 | 0.03 | 0.23 | 0.73 | 0.62 | 19.86 | 0.02 | 0.68 | 0.01 | 0.19 | 96.74 | 0.06 | - | - | 7.85 | - | - | 0.16 | - | 0.02 |
| HS11 | 9.13 | 8.17 | 13.04 | 0.02 | 0.18 | 0.64 | 2.58 | 134.71 | 0.03 | 2.05 | 0.01 | 0.36 | 263.61 | 0.02 | 0.01 | 0.01 | 22.37 | 0.001 | - | 0.11 | - | 0.53 |
| HS12 | 7.37 | 28.55 | 23.54 | 0.03 | 0.30 | 1.24 | 2.51 | 49.33 | 0.14 | 5.73 | 0.05 | 0.14 | 34.78 | 0.09 | - | - | 38.75 | - | - | 0.18 | 0.001 | 0.03 |
| HS13 | 14.94 | 10.65 | 10.86 | 0.02 | 0.47 | 0.60 | 15.09 | 805.45 | 0.07 | 1.27 | 0.05 | 0.96 | 592.95 | 0.02 | 0.01 | 0.01 | 146.07 | - | - | 0.17 | - | 1.01 |
| HS14 | 183.76 | 17.48 | 7.06 | 0.07 | 0.14 | 2.50 | 2.94 | 12.72 | 0.04 | 11.66 | 0.00 | 11.25 | 3244.88 | 0.02 | 0.02 | 0.01 | 92.96 | 0.001 | 0.01 | 0.10 | 0.001 | 0.34 |
| HS15 | 4.34 | 5.41 | 6.85 | 0.03 | 0.19 | 0.03 | 0.69 | 14.15 | 0.01 | 0.32 | 0.00 | 1.86 | 30.13 | 0.01 | - | - | 2.36 | - | - | 0.15 | - | 0.01 |
| HS16 | 491.19 | 6.67 | 812.91 | 0.03 | 0.29 | 7.20 | 0.89 | 34.78 | 0.10 | 10.68 | 0.00 | 2.23 | 738.82 | 0.02 | 0.02 | - | 39.83 | 0.001 | 0.01 | 0.20 | 0.002 | 5.08 |

Note: "-" represents below detection limit or undetected. Hf and Ta are kept to 3 decimal places due to their low content.

## 5 Discussion

### 5.1 The origin of groundwater in different segments of EAFZ

Previous studies have documented abundant geothermal resources within the EAFZ, which is characterized by low or moderate temperature geothermal systems (Aydin et al., 2020; Baba et al., 2019). Both aqueous and gaseous geochemical signatures indicate mixing between deep-sourced mantle/crustal fluids and shallow groundwater reservoirs (Aydin et al., 2020; Italiano et al., 2013; Yuce et al., 2014). Yuce et al. (2014) proposed that geothermal fluids at the southwest end of the EAFZ are triggered by deep-rooted regional faults, with localized seawater intrusion. Analogously, there are deep components involved in the geothermal fluid circulation in the middle to east section of EAFZ. However, the source of deep components are thought to be controlled by magmatic activity rather than from deep-rooted regional faults (Aydin et al., 2020; Italiano et al., 2013; Karaoğlu et al., 2019). At the intersection of the EAFZ and the North Anatolian Fault Zones (NAFZ), which is also known as the Karliova triple junction, there is extensive volcanic activity that may have provided energy and components for the geothermal fluid cycle eastern segment of the EAFZ (Bilim et al., 2018; Karaoğlu et al., 2018; Karaoğlu et al., 2020). Furthermore, Italiano et al. (2013) suggested these volcanic activities may even contribute to geothermal fluids in the middle segment of the EAFZ. These findings collectively suggest multiple tectonic controls (volcanism, fault activity, and seawater intrusion) on EAFZ's geothermal systems.

The February 2023 earthquake sequence (*Mw* 7.8 and 7.6) ruptured the central EAFZ segment. A critical question arises: Are the observed pre-seismic groundwater anomalies seismogenically linked to this seismic event? To address this, we conducted comparative analyses of post-seismic hydrochemical data against a decadal-scale (13-year) pre-seismic groundwater dataset, as detailed below:

#### 5.1.1 Hydrogen and oxygen isotope characteristics of groundwaters

Hydrogen and oxygen isotopes serve as robust geochemical tracers for elucidating the origin of geothermal fluids groundwater. As illustrated in Fig. 3, the δD and $\delta^{18}O$ compositions of groundwater in the EAFZ align closely with the GMWL (Craig, 1961), indicating predominant atmospheric precipitation recharge. Notably, groundwater in the southern EAFZ proximal to the Mediterranean Sea exhibits progressively heavier isotopic signatures toward the coast, consistent with recharge sourced from evaporated Mediterranean seawater. In contrast, northern groundwater displays distinct $\delta^{18}O$ enrichment deviating from local meteoric trends, indicative of mixing with deep-sourced magmatic fluids—a interpretation corroborated by widespread Quaternary volcanic activity in the northern sector (Fig. 3) (Bilim et al., 2018; Karaoğlu et al., 2018; Karaoğlu et al., 2020). Conversely, central and southern groundwater samples exhibit isotopic signatures decoupled from magmatic inputs, reflecting the absence of active deep-seated magma reservoirs in these segments.

### 5.1.2 Major ion characteristics of groundwaters

The groundwater chemistry exhibits distinct spatial heterogeneity across the EAFZ segments. Northern groundwaters are significantly enriched in $Na^+$, $K^+$, and $Cl^-$ (Na-Cl and Na-$HCO_3$ type), whereas central and southern segments display Ca-Mg-$HCO_3$ type waters, with localized Ca-$SO_4$ and Na-Cl anomalies (Fig. 2). These hydrochemical disparities likely reflect fundamentally distinct recharge sources and circulation pathways.

As discussed earlier, magmatic fluid contributions are evident in northern groundwaters. Chloride serves as a key tracer for magmatic input (Luo et al., 2023; Pan et al., 2021). In the eastern EAFZ, $Cl^-$ concentrations span 0.4–2500 mg/L, markedly higher than central/southern values. Given the segment's inland setting, seawater intrusion is negligible, suggesting $Cl^-$ enrichment primarily originates from magmatic fluids. Notably, $Na^+/Cl^-$ molar ratios deviate from theoretical mixing trends, with $Na^+$ excesses implicating additional sodium sources (e.g., albite dissolution), to be detailed in Section 5.2. This interpretation aligns with petrological and geophysical evidence of active magmatism in the eastern EAFZ (Bilim et al., 2018; Karaoğlu et al., 2018; Karaoğlu et al., 2020; Maden and Öztürk, 2015; Oyan, 2018). Integrated H-O isotopic, major ion, and volcanic activity data collectively support a mixing model between meteoric water and magmatic fluids in the northern EAFZ.

In contrast, central and southern groundwaters exhibit lower $Na^+$ and $Cl^-$ concentrations, with sporadic anomalies attributable to evaporite dissolution or limited seawater influence (Table 1). The Ca-Mg-$HCO_3$ dominance, coupled with isotopic signatures, reflects shallow circulation systems (<5 km depth) devoid of significant deep tectonic/magmatic inputs (Table S2). $Ca^{2+}$ likely derives from calcite, dolomite, or plagioclase weathering, while $Mg^{2+}$ sources include dolomite and serpentinite. Pre-seismic turbidity at HS14 (Video 1) may indicate earthquake-induced disruption of water-rock equilibria.

However, the geothermal gases in the centre and south segment of EAFZ exhibit mantle-like $\delta^{13}C_{CO_2}$ (−5.6‰ to −0.2‰) and elevated $^3He/^4He$ ratios (Rc/Ra = 0.44–4.41), contrasting with the absence of deep fluid signatures in groundwater (Italiano et al., 2013). Actually, this decoupling results from fundamentally distinct migration mechanisms. Groundwater circulation operates as a shallow crustal system dominated by meteoric recharge, structurally confined by fault architecture. Conversely, geothermal gases predominantly represent deep-seated fluids, with their high mobility and low density enabling efficient ascent through fractures. This explains why mantle/crustal signals are preserved in gases but attenuated in aqueous phases.

To further constrain groundwater source area, we have calculated the thermal reservoir temperature of EAFZ groundwater, and the results are shown in Table S2. Due to the low water-rock interaction degree and diversity of rock types in this area, cations in water are difficult to reach water-rock equilibrium (Fig. 4). Hence, most of the cationic thermometer estimates are too large or too small, which can only be used as a reference for thermal reservoirs. Fortunately, $SiO_2$ thermometers are relatively suitable for estimating the reservoir temperature. As can be seen from Table S2, the reservoir temperatures range from 19.81°C to 128.09 °C (Quartz, no steam loss), which belongs to the low or moderate temperature geothermal systems. Using the circulation depth calculation formula, the maximum circulation depth is estimated to be 4.4km (HS04) (Table S2).

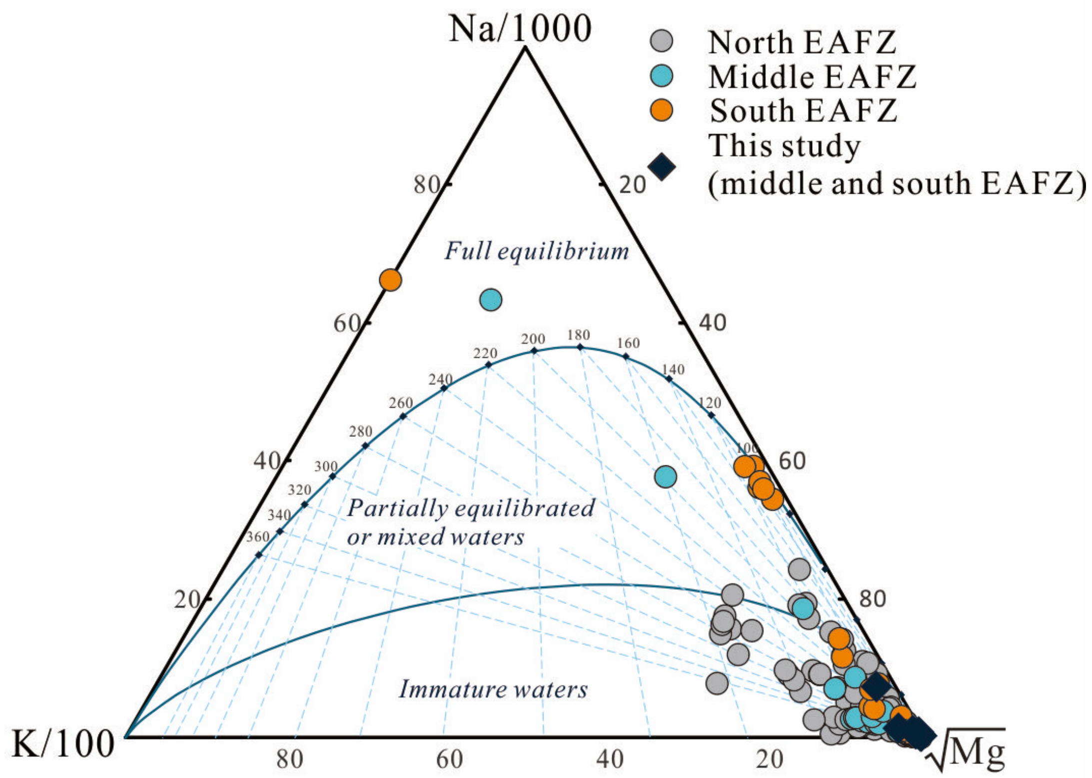


**Fig. 4. Na-K-Mg ternary diagram of groundwaters in EAFZ. Literature data source is consistent with Fig. 2.**

### 5.1.3 $^{87}Sr/^{86}Sr$ characteristics of groundwaters

Radiogenic strontium isotopes ($^{87}Sr/^{86}Sr$) serve as robust tracers of groundwater provenance. The measured $^{87}Sr/^{86}Sr$ ratios (0.7053–0.713) across EAFZ groundwaters reflect multi-source mixing processes. Central-southern groundwaters integrate signatures from: Shallow aquifers: Inheriting Sr from local lithologies (ophiolites) (Oyan, 2018); Modern seawater: $^{87}Sr/^{86}Sr$ = 0.7092–0.7096 (Mediterranean seawater) (Banner, 2004; Bernat et al., 1972); River inputs: Enriched ratios (>0.710) from silicate weathering. Binary mixing models using $^{87}Sr/^{86}Sr$ vs. Ca/Sr ratios (Fig. 5) quantify source contributions: Carbonate weathering dominates, consistent with $Ca\text{-}HCO_3$ hydrochemical type; Ophiolite contributions <10% (except $Mg^{2+}$-rich samples near ultramafic outcrops); Evaporite dissolution contributes 0–20% (≤50% in localized high-$SO_4^{2-}$ zones). Sr isotope framework corroborates earlier findings of shallow-dominated circulation in central-southern EAFZ.

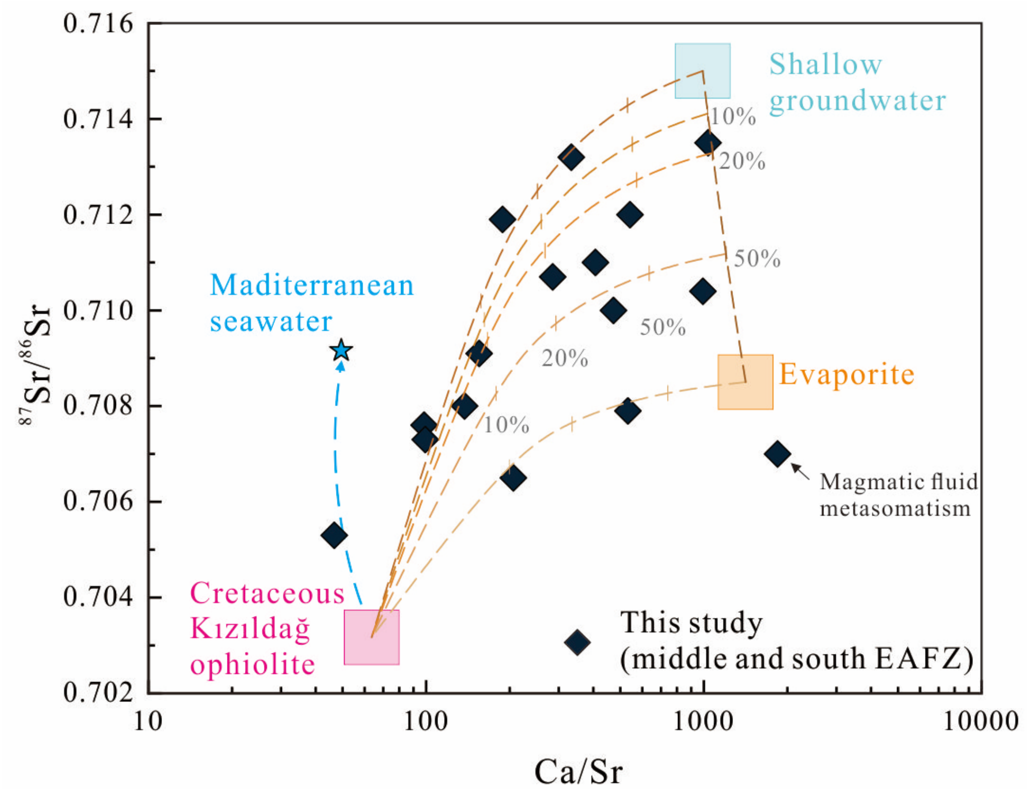


**Fig. 5. $^{87}Sr/^{86}Sr$ vs. Ca/Sr of groundwaters in the EAFZ. The mixing-boundary lines are built with the following end members: Mediterranean Sea water Ca = 411ppm, Sr = 8.30ppm $^{87}Sr/^{86}Sr$ = 0.7092 (Banner, 2004; Bernat et al., 1972); Cretaceous Kızıldağ ophiolite CaO = 9.7%, Sr = 1088.10ppm $^{87}Sr/^{86}Sr$ = 0.7032 (Oyan, 2018); Shallow groundwater (HS08) Ca = 55.34ppm, Sr = 0.06ppm $^{87}Sr/^{86}Sr$ = 0.7150 (Affected by silicate weathering); Evaporite CaO = 29.5%, Sr = 149ppm $^{87}Sr/^{86}Sr$ = 0.7085 (Güngör Yeşilova and Baran, 2023).**

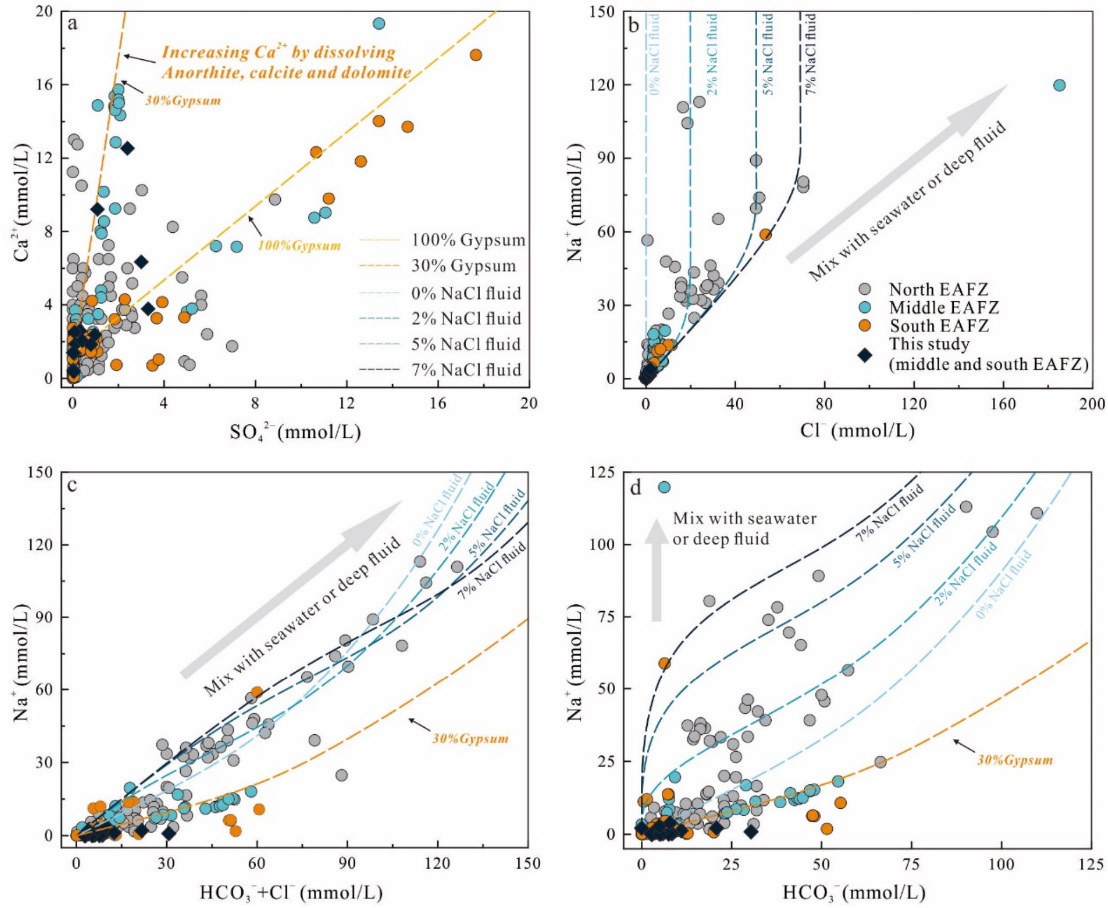


**Fig. 6. Characteristics of chemical components of groundwaters in the EAFZ, during water-rock interaction. The dashed line is the numerical simulation result of PHREEQC. a: $Ca^{2+}$ vs $SO_4^{2-}$, b: $Na^+$ vs $Cl^-$, c: $Na^+$ vs $HCO_3^-$+$Cl^-$ and d: $Na^+$ vs $HCO_3^-$. The simulation calculations are detailed in Supporting Information Part 1. Literature data source is consistent with Fig. 2.**

## 5.2 The groundwater circulation in different segments of EAFZ

### 5.2.1 Water-rocks interaction

Pre-seismic whitish discoloration and turbidity anomalies observed at HS04 and HS14 groundwater monitoring stations likely reflect seismically induced perturbations to water-rock equilibrium (Video 1 and 2). To validate this hypothesis, we conducted numerical simulations of water-rock interaction processes across distinct segments of EAFZ, aiming to reconstruct their hydrochemical evolution.

Fig. 6 indicates pronounced disparities in groundwater chemistry between northern and central-southern segments. As discussed, elevated $Na^+$ and $Cl^-$ concentrations in northern groundwaters suggest magmatic fluid contributions. During ascent, these deep-sourced Na-Cl rich fluids mix with shallow groundwater while reacting with surrounding rocks. To quantify magmatic mixing ratios and reaction pathways, we first characterized dominant lithologies in the northern EAFZ—basalt, basaltic andesite, and sedimentary cover (clastics and carbonates). CIPW norm calculations were employed to estimate mineral abundances, followed by PHREEQC-based reactive transport modeling (Parkhurst and Appelo, 2013) (see Supplementary File 1 for parameters). Simulation results (Fig. 6) demonstrate that linear correlations between $Na^+$ and ($HCO_3^-$+ $Cl^-$) arise from magmatic NaCl fluid-carbonate interactions, with magmatic contributions accounting for 0–7% of total mixing.

In contrast, central−southern groundwaters lack magmatic signatures but exhibit $Ca^{2+}$−$SO_4^{2-}$ covariation indicative of anhydrite dissolution (Fig. 6). Central segment waters reflect mixed carbonate- anhydrite controls (30% anhydrite contribution), while southern systems are dominated by anhydrite-derived solutes (100%), sourced from extensive evaporite deposits of the paleo−Amik Lake. Silica−enthalpy mixing models estimate reservoir temperatures of 234°C (HS04) and 155°C (HS04) (Fig. 7a), under which anhydrite saturation indices confirm its dissolution dominance (Fig. 7b). Notably, HS14—located 20 km from the paleo−Amik Basin—displayed prominent pre-seismic turbidity anomalies, likely triggered by earthquake-driven disruption of anhydrite equilibrium. Coseismic changes in temperature, pressure, fracture density, and circulation depth may have enhanced evaporite dissolution, increasing groundwater salinity.

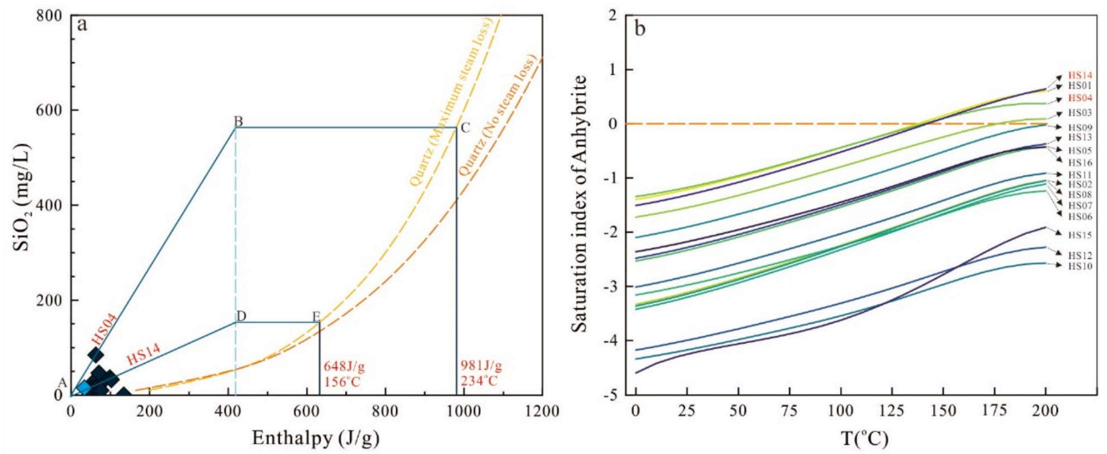


**Fig. 7. a: Silica-enthalpy model of groundwaters in EAFZ. b: Temperature versus variation of anhydrite saturation indices of groudwaters in EAFZ. The enthalpies and reservoir temperatures of sample HS04 and HS14 are 981 J/g, 234 °C and 648 J/g, 156 °C respectively. The blue diamond is sample HS08, which is river water. At reservoir temperature, the anhydrite in HS04 and HS14 samples is saturated, indicating that anhydrite dissolution occurs during the water-rock reaction.**

5.2.2 Contribution of mantle degassing to EAFZ groundwater circulation

Geochemical studies of EAFZ geothermal gases indicate significant mantle degassing (Fig. 8), where sulfur volatiles (e.g., $SO_2$ and $H_2S$) ascend through fault conduits and oxidize upon mixing with shallow groundwater, ultimately mobilizing as $SO_4^{2-}$ in thermal fluids. Consequently, mantle-derived sulfur contributions to groundwater sulfate inventories cannot be disregarded. Lacking $O_2$ was detected in EAFZ geothermal gases suggested that the dissolved oxygen may have been consumed (Italiano et al., 2013; Yuce et al., 2014). However, it is important to note that $H_2S$, $H_2$, and $CH_4$ can all react with oxygen. Thermodynamic calculations indicate that $CH_4$ is more favorable than $H_2S$ in oxidation reactions ($\Delta G°$ $CH_4$ = -818.1 kJ/mol, $\Delta G°$ $H_2S$ = -494.2 kJ/mol, at 298 K and 1atm). In actual geothermal systems, however, the depletion of $H_2S$ is more commonly observed than the depletion of $CH_4$. We propose the following possible explanations: 1) Oxidation of $H_2S$: While thermodynamic calculations predict $CH_4$ oxidation first, a small amount of $H_2S$ might still be oxidized simultaneously with $CH_4$. Due to the much lower concentration of $H_2S$ in geothermal systems compared to $CH_4$, $H_2S$ is consumed more quickly, leaving $CH_4$ with a higher residual concentration. 2) Exogenous $CH_4$ Supply: In addition to mantle-derived $CH_4$, other sources of $CH_4$, such as biogenic $CH_4$ and thermogenic $CH_4$ (e.g., serpentinization), may contribute to the geothermal system. These external sources could increase the concentration of $CH_4$ in the geothermal fluids.

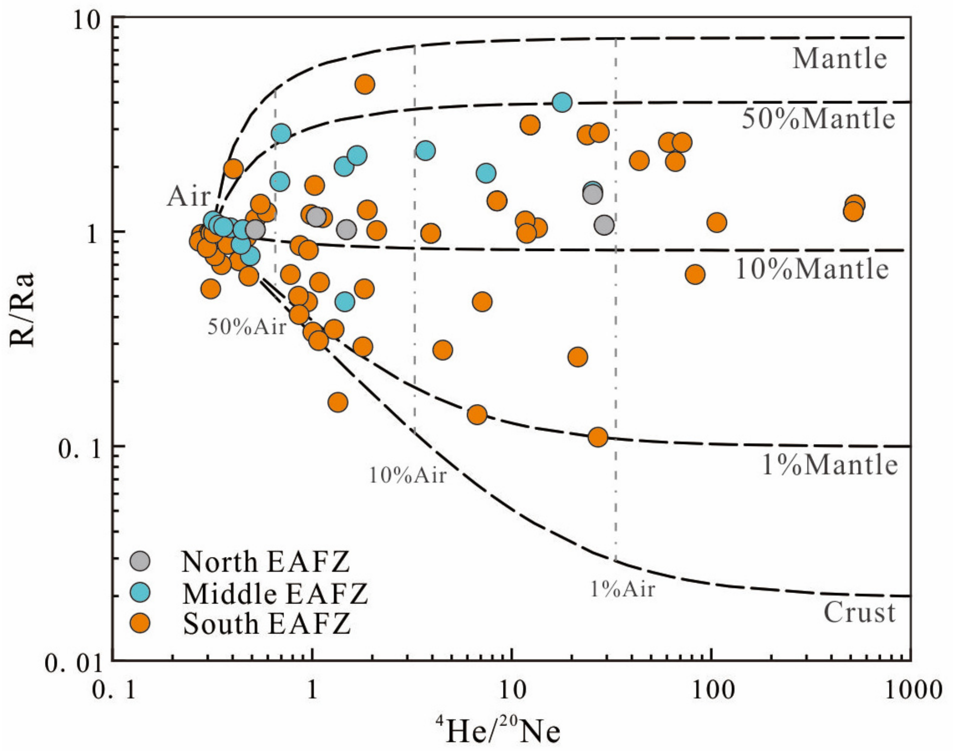


**Fig. 8. Helium isotope ratios (R/Ra, Ra = air $^3He/^4He = 1.39 \times 10^{-6}$) versus $^4He/^{20}Ne$ ratios for EAFZ gas samples. The mixing-boundary lines are built with the following end members: Air R/Ra = 1 and $^4He/^{20}Ne$ = 0.318; mantle R/Ra = 8 and $^4He/^{20}Ne$ = 1000; continental crust R/Ra = 0.02 and $^4He/^{20}Ne$ = 1000 (Sano and**

**Wakita, 1985). Literature data source from (D'Alessandro et al., 2018; Inguaggiato et al., 2016; Italiano et al., 2013; YASİN and YÜCE, 2023; Yuce et al., 2014; Yuce and Taskiran, 2013).**

However, previous studies have shown that the geothermal gas in the southern segment of EAFZ has more crustal source components than northern segment (Fig. 8). Furthermore, isotopic evidence confirms substantial biogenic and serpentinization-derived $CH_4$ inputs (Italiano et al., 2013; Yan et al., 2024), whereas $H_2S$ remains below detection thresholds. This implies that while $H_2S$ may transiently influence redox cycling, its low abundance limits long-term impacts. Instead, post-seismic $SO_4^{2-}$ surges likely originate from shallow evaporite dissolution (anhydrite) or low-temperature metamorphic anhydrite hydration—processes amplified by coseismic fracture propagation and fluid remobilization. ~~*5.1 The origin of geothermal fluids*~~

~~Hydrogen and oxygen isotopes are effective geochemical indexes for tracing the origin of geothermal fluids. It can be seen from Fig. 3 that the hydrogen and oxygen isotopes of the sample have obvious positive correlation. Combined with the geothermal fluid data of EAFZ in the literatures, the correlation between the hydrogen and oxygen isotopes is $\delta D = 8.48\ \delta^{18}O+17.87$ ($R^2$=0.95, n=110), which is consistent with the global meteoric water line (GMWL) (Craig, 1961) (Fig.3), suggesting that these geothermal fluids are controlled by meteoric water. "Oxygen drift" is not obvious, indicating that the degree of water-rock interaction in the geothermal fluid cycle is limited and/or the oxygen isotope composition of the fluid and rock is indiscriminately (However, given the complex and diverse lithology of EAFZ, the latter is highly unlikely) (Fig. 1). The highest value of δD ( 6.55‰) and $\delta^{18}O$ ( 34.43‰) at the southwest end of EAFZ, which is close to the Mediterranean Sea, indicating that it originates from the recharge of the evaporation of the Mediterranean Sea (Fig.3). Due to the influence of the continent and altitude, the farther away from the coastline, the lighter the hydrogen and oxygen isotopic composition.~~

Geothermal fields are generally distributed along the EAFZ, which is characterized by low or moderate temperature geothermal systems (Aydin et al., 2020; Baba et al., 2019). Previous studies pointed out that both water and gas characteristics indicate that geothermal fluids is a mixture of shallow and deep components either of mantle and crustal origin (Aydin et al., 2020; Italiano et al., 2013; Yuce et al., 2014). Yuce et al. (2014) argue that geothermal fluids at the southwest end of the EAFZ are triggered by deep-rooted regional faults. Analogously, there are deep components involved in the geothermal fluid circulation in the middle to east section of EAFZ. However, the source of deep components are thought to be controlled by magmatic activity rather than from deep-rooted regional faults (Aydin et al., 2020; Italiano et al., 2013; Karaoğlu et al., 2019). At the intersection of the EAFZ and the North Anatolian Fault Zones (NAFZ), which is also known as the Karliova triple junction, there is extensive volcanic activity that may have provided energy and components for the geothermal fluid cycle eastern segment of the EAFZ (Bilim et al., 2018; Karaoğlu et al., 2018; Karaoğlu et al., 2020). Furthermore, Italiano et al. (2013) suggested these volcanic activities may even contribute to geothermal fluids in the middle segment of the EAFZ.

$Na^+$ and $Cl^-$ are often used as a reference when judging whether there is magma mixing in geothermal fluids (Luo et al., 2023; Pan et al., 2021). In the eastern section of EAFZ, the concentration of $Na^+$ (1.3~2600mg/L) and $Cl^-$ (0.4~2500 mg/L) varies widely (Aydin et al., 2020). In the case of excluding the mixing of halite and seawater (Luo et al., 2023; Wei et al., 2021), it is possible that there is contaminated by magmatic fluid. Petrological and geophysical observations also support magmatic activity in the eastern section of EAFZ (Bilim et al., 2018; Karaoğlu et al., 2018; Karaoğlu et al., 2020; Maden and Öztürk, 2015). Furthermore, Italiano et al. (2013) suggested that $\delta^{13}C_{CO2}$ (-5.6‰~-0.2‰) and He (Rac (values corrected for the atmospheric contamination) = 0.44~4.41) revealed a fluid of mantle-derived in the middle segment of the EAFZ. However, the $Na^{+}$ (0.42~88.93 mg/L) and $Cl^{-}$ (0.97~75.92 mg/L) of the samples in this study were both low. HS16, the sample with the highest concentration, was collected at the southwest of EAFZ, which was obviously contaminated by Mediterranean Sea water and had no signal of deep fluid or magma source. This is not consistent with the previous study. Furthermore, the gas and water cycles appear to be decoupled in the EAFZ. We suggest that the reason for the inconsistency may be controlled by two factors: 1) After the earthquake, dislocation movement occurred in the fault zone, resulting in a large amount of surface water and shallow groundwater infiltration, which diluted the geothermal fluid; 2) The origin and evolution of geothermal water and geothermal gas are different. The cycle of geothermal water is essentially a cycle in the upper crust dominated by precipitation and controlled by fault zones. Nevertheless, geothermal gas is dominated by deep fluid, with a little or no air pollution. In addition, the strong fluidity and low density of gas make it easier to removal than water, which makes deep geothermal fluids may not be able to rise along the fault to the shallow crust or surface like geothermal gas. Although there is an obvious signal of deep crust or mantle in geothermal gas, the signal of deep crust or mantle is lacking in geothermal water. Therefore, we argue that the gas and water cycles may be decoupled in the EAFZ, with the gas more responsive to deep information than the water.

Since the deep information is lacking in geothermal water, it can still be used to trace shallow geothermal fluid cycles. Geothermal reservoir temperature estimation is one of the important indicators to understand the geothermal water cycle. We have calculated the thermal reservoir temperature of EAFZ geothermal water, and the results are shown in Table S1. Due to the low water-rock interaction degree and diversity of rock types in this area, cations in water are difficult to reach water-rock equilibrium (Fig. 4). Hence, most of the cationic thermometer estimates are too large or too small, which can only be used as a reference for thermal reservoirs. Fortunately, $SiO_2$ thermometers are relatively suitable for estimating the reservoir temperature. As can be seen from Table S1, the reservoir temperatures range from 19.81°C to 128.09 °C (Quartz, no steam loss), which belongs to the low or moderate temperature geothermal systems. Using the circulation depth calculation formula, the maximum circulation depth is estimated to be 4.4km (HS04) (Table S1). It is very close to the epicenter of the 2023 *Mw* 7.6 earthquake (Fig. 1).

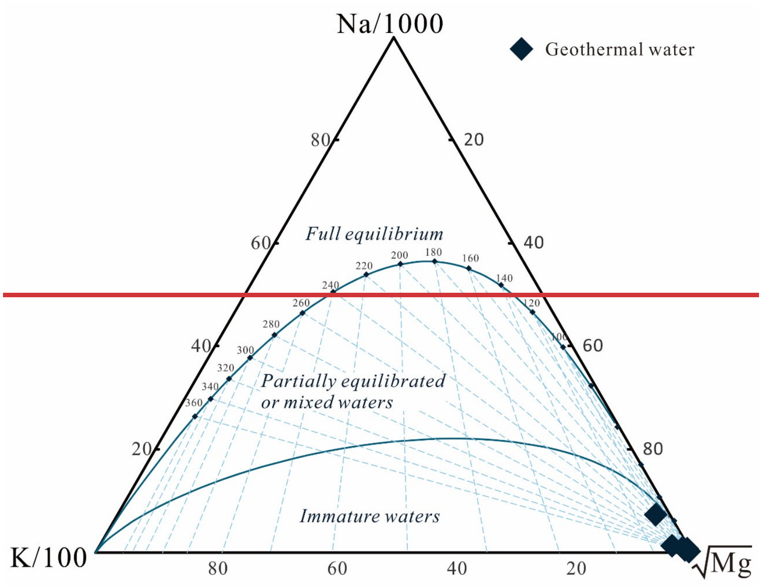


Figure 4. Na-K-Mg ternary diagram of geothermal waters in EAFZ.

As mentioned above, deep geothermal fluid may be diluted by shallow cold water. The silicon-enthalpy model is an effective tool to evaluate and eliminate the effects of the cold water mixing (Fournier, 1977). It can be seen from the Fig. 5a that HS04, which is closest to the epicenter, has the highest reservoir temperature (234 °C) indicating that the earthquake did break the balance of water-rock interaction in the EAFZ and released more deep materials and energy. Furthermore, we applied the $Cl^-$–enthalpy model to constrain the potential deep geothermal fluid. Fig. 5b suggests that the temperature of the deep geothermal fluid is 382 °C. Such high temperatures are further evidence of the effect of seismic activity on geothermal fluid circulation.

Therefore, after analysing the data of this study, we suggest that the double earthquakes in February 2023 (*Mw* 7.8 *and Mw* 7.6) modified geothermal fluid in the EAFZ, including: materials and energy. The maximum heat storage temperature and maximum circulation depth of geothermal water are 128 °C and 4.4km respectively. The temperature of the deep geothermal fluid is 382 °C. Although the deep fluid modified the geothermal fluid, the geothermal fluid was diluted due to the infiltration of a large amount of shallow cold water after the earthquake, and the information of the deep fluid was eventually occulted.

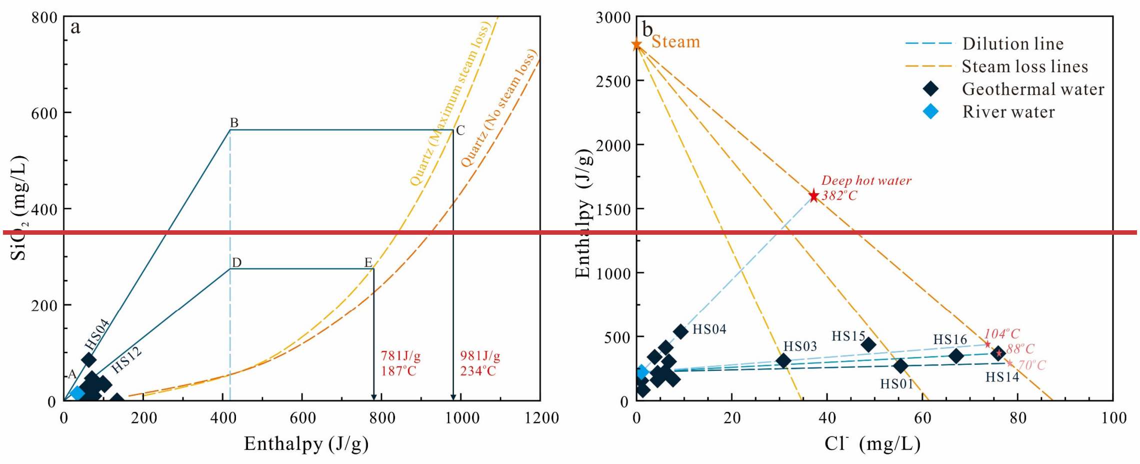


Figure 5. a: Silica-enthalpy model of geothermal waters in LXF zone. b: Enthalpy and $Cl^-$ concentration diagram for identifying the deep hot water in EAFZ. The enthalpies and reservoir temperatures of sample HS04 and HS12 are 981 J/g, 234 °C and 781 kJ/kg, 187 °C respectively. Steam point with enthalpy value of 2779.4 J/g and chloride concentration of 0 mg/L (Kretzschmar and Wagner, 2019). The blue diamond is sample HS08, which is river water. HS04 is the closest sampling point to the epicenter, and the temperature of its deep fluid is as high as 382 °C.

*5.2 Water-rocks interaction*

As shown in Fig. 3 and 4, the water-rock interaction of the geothermal water is weakly. Nevertheless, we still find chemical composition anomalies in a few samples. Geothermal water samples collected at SF (Sürgü Fault) have higher EC (286.5~2683μs/cm) and ion concentrations, such as $Ca^{2+}$ (54.04~501.58mg/L), $Mg^{2+}$ (6.58~116.20mg/L), and $SO_4^{2-}$ (6.37~287.74mg/L) (Table 1). We arranged the samples collected by EAFZ in the order from northeast to southwest, and the results are shown in Fig. 6. All samples show weak alkalinity (pH=8.11~8.50) except HS15 (pH=11.72). Natural waters with high pH (~ 10 or above) are not usual (Hem, 1985). We suspect that there are two processes that may cause pH to increase: 1) Serpentinization of olivine in ultramafic terranes (Huang; et al., 2023), 2) Secondary mineral precipitation, such as: calcite or magnesite (Aydin et al., 2020; Cipolli et al., 2004). Compared with other samples, the ion concentration of HS15 is significantly reduced, which may indicate the precipitation of potential secondary minerals (e.g., calcite). Therefore, we suggest that process 2 May be the dominant factor leading to the increase of pH.

The $Na^+$ and $Cl^-$ contents of the samples remained stable and only showed significant positive anomalies near the southwestern end of the Mediterranean Sea, which was caused by seawater pollution (HS14, HS15 and HS16) (Fig. 6d). The low content and spatial stability of $Na^+$ (0.84~7.66mg/L) and $Cl^-$ (0.897~7.67mg/L) and the co-variation of hydrogen and oxygen isotopes (Fig. 6c, d), indicating that exogenous $Na^+$ and $Cl^-$ are not involved in the geothermal water cycle in EAFZ observably (e.g., mantle or magma). In combination with the discussion in section 5.1, we suggest that the low $Na^+$, $Cl^-$ content is the result of dilution by a large amount of shallow cold water.

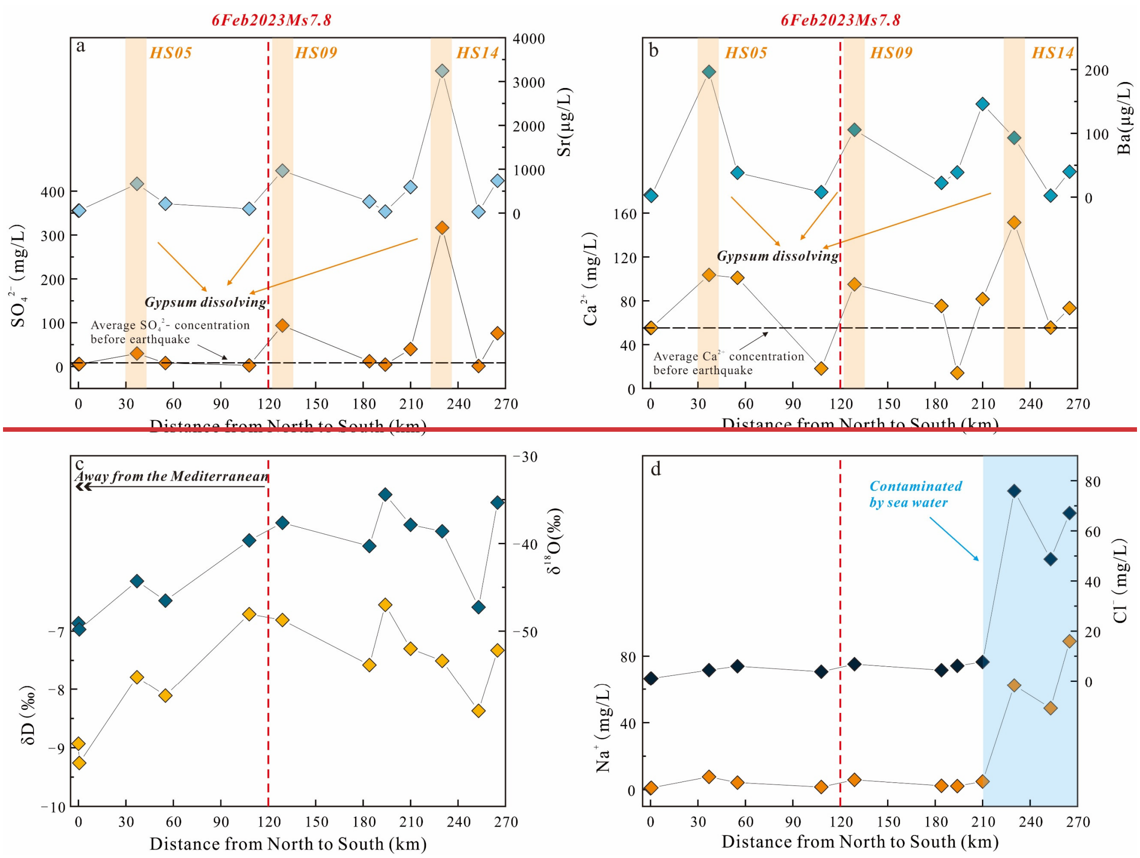


~~Figure 6. Spatial distribution characteristics of geothermal water in EAFZ after the February 2023 double earthquakes in Turkey. Horizontal coordinate: Starting with the first sample (HS07) at the northeast end, it is distributed in the southwest direction along the EAFZ. From northeast to southwest, they are HS07, 08, 05, 06, 10, 09, 11~16. The number indicates the distance from the HS07 sample. The higher the abscissa, the closer it is to the Mediterranean. Average $Ca^{2+}$ (55.23 mg/L) and $SO_4^{2-}$ (8.31 mg/L) concentrations before earthquake in the EAFZ from Baba et al. (2019).~~

~~EAFZ geothermal waters are controlled by shallow circulation. Therefore, the shallow sedimentary cover may be the main factor in the geochemical composition of the modified geothermal waters. We observed positive abnormalities of $SO_4^{2-}$ (2.76~316.61mg/L), $Ca^{2+}$ (14.16~151.43mg/L), Sr (34.78~3244.8μg/L), and Ba (1.89~196.48μg/L) in at least three locations synergistically (HS05, HS09, HS14) (Fig.~~

6). Apparently, it is due to the dissolution of gypsum. The extensive distribution of evaporative rock layers in EAFZ provides geological evidence for this hypothesis (Aydin et al., 2020; Italiano et al., 2013; Yuce et al., 2014). In particular, HS14 is located near Ancient Amik Lake, and there were macroscopic anomalies such as white water and turbidity before the earthquake, which further verified that the anomalies originated from the dissolution of gypsum (Fig. S1). Furthermore, the $Mg^{2+}$ concentrations of our samples varied from 0.38mg/L to 116.2mg/L, and such a large change may imply the dissolution of Mg-containing minerals, which will be discussed in detail later.

In order to accurately evaluate the cycle process of EAFZ geothermal water, PHREEQC software was used to conduct quantitative simulation of the water-rock interaction process (The simulation calculation process is detailed in Supporting Information) (Parkhurst and Appelo, 2013). The results are shown in Fig. 7. HS05, HS09 and HS14 are consistent with the simulated dissolution curves of 100% gypsum, which confirms our conjecture about the dissolution of gypsum (Fig. 7a). Incidentally, the dissolution curves of celestite ($SrSO_4$) and barite ($BaSO_4$) have also been simulated. HS05 and HS09 may also be affected by the dissolution of barite, while HS14 may also be affected by the dissolution of celestite (Fig. 7b). HS01, HS03, and HS04 have excessive $Ca^{2+}$ concentrations, indicating that other minerals besides gypsum are involved in the water-rock interaction process and provide Ca (Fig. 7a). After investigating the types of rocks in the study area, we found that in addition to gypsum, other Ca-bearing minerals, such as calcite ($CaCO_3$), dolomite ($CaMg(CO_3)_2$), and Anorthite ($CaAl_2Si_2O_8$), may be involved in the water-rock interaction process. When the ratio of calcite: dolomite : Anorthite = 1:1:1, the simulated results of $Ca^{2+}$ and $HCO_3^-$ are consistent with the observed values, indicating that the three minerals participate in the water-rock interaction in equal proportion (Fig. 7c). Furthermore, HS03 and HS04 have higher ion concentrations than HS01, possibly because HS03 and HS04 are closer to the epicentre of 2023 *Mw* 7.6 earthquake (Fig. 1).

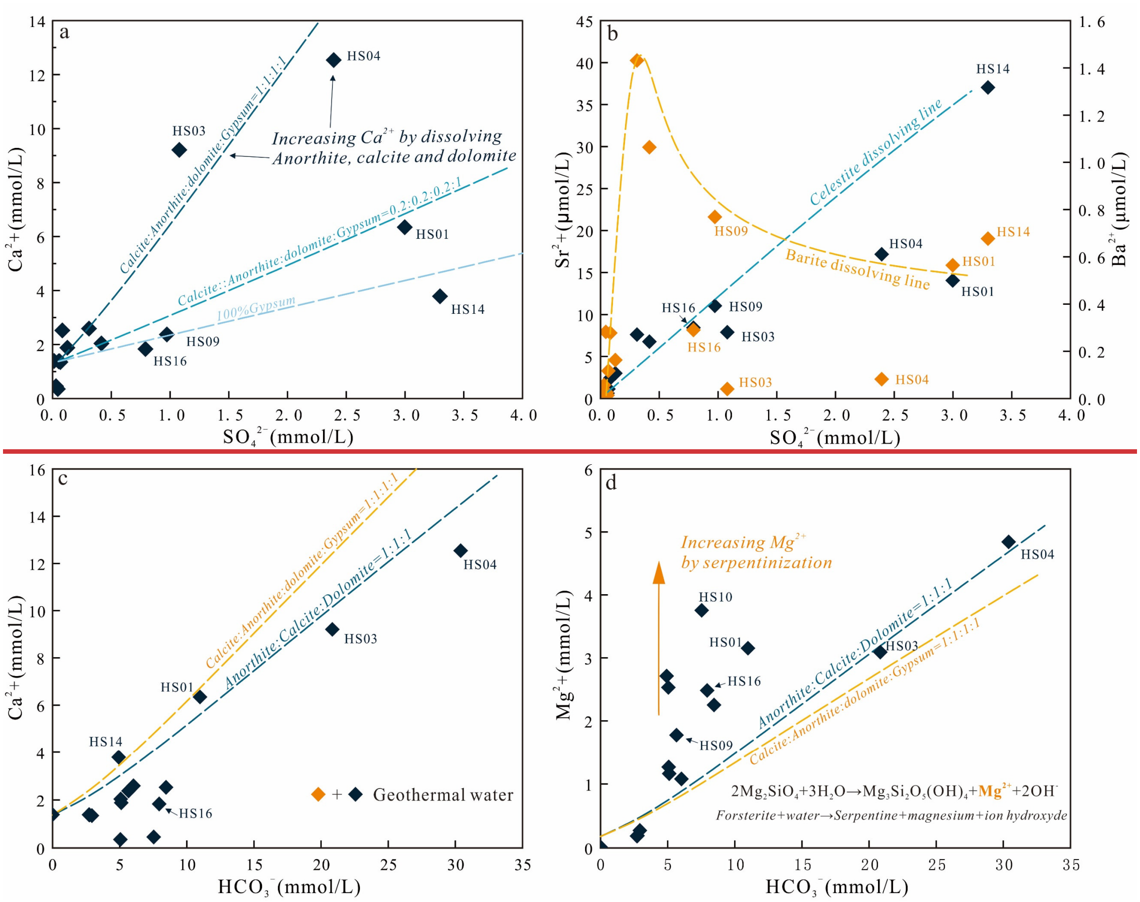


Figure 7. Characteristics of chemical components of geothermal waters in the EAFZ, during water-rock interaction. The diamond is the measured value of geothermal waters. The dashed line is the numerical simulation result of PHREEQC. a: $Ca^{2+}$ vs $SO_4^{2-}$, b: $Sr^{2+}$ and $Ba^{2+}$ vs $SO_4^{2-}$, c: $Ca^{2+}$ vs $HCO_3^-$ and d: $Mg^{2+}$ vs $HCO_3^-$. The simulation calculations are detailed in Supporting Information.

It is worth noting that the $Mg^{2+}$ concentrations in the samples are generally high (0.38~116.2mg/L). It can also be seen from the simulation results that only dolomite provides Mg is not enough to explain the variation of $Mg^{2+}$ concentrations in the sample (Fig. 7d). Actually, considering that the study area is located in the Alpine-Himalayan suture zone, there are a large number of ultrabasic rocks and basic rocks distributed in the region (Fig. 1), which provide the main Mg source for geothermal water (Lanari et al., 2023; Sparacino et al., 2022; van Hinsbergen et al., 2024). Serpentinization of peridotite is the main reason for controlling the variation of Mg content in geothermal water (Fig. 7d) (Aydin et al., 2020; Huang; et al., 2023).

In short, through the analysis of the chemical components of geothermal water and the simulation calculation, we mainly obtained the following understandings: 1) The change of $Na^{+}$ and $Cl^{-}$ concentration in the samples was caused by the mixing of Mediterranean Sea water; 2) Gypsum dissolution exists in geothermal fluids (HS05, HS09 and HS14); 3) $Ca^{2+}$ originated from gypsum, calcite and anorthite; 4) Serpentinization is the main factor controlling $Mg^{2+}$ concentrations.

*5.3 Geothermal fluid circulation model in the EAFZ*

As discussed above, EAFZ's geothermal fluid circulation model is shown in the Fig. 8. Beginning in the Late Cretaceous, as the New Tethys Ocean closed, Arabia-Eurasia collision zone have accommodated ~350 km of convergence, making crust up to 45 km thick, and causing >2 km of uplift (Yönlü et al., 2017). Arabian lithospheric mantle extends 50~150 km north beneath Anatolian crust (Whitney et al., 2023). Subsequently, the “roll back” and “slab break” occurred, resulting in extensive volcanic and devastating earthquakes, including those of February 6, 2023 in East Anatolian Plateau (Zhou et al., 2024). The collision of the Eurasian and Arabian plates caused Anatolian microplate was extruding westwards, which lead to EAFZ at a high strike-slip rate of ~11 mm/yr (Pousse‐Beltran et al., 2020), and accompanied by counterclockwise rotation with a rotation rate of 1.053 ±0.015°/Ma (Simão et al., 2016). In this tectonic context, EAFZ remains active for a long time. Paleoseismic studies have shown that EAFZ has had many large earthquakes in its history (Carena et al., 2023; Hubert-Ferrari et al., 2020; Sparacino et al., 2022; Tan et al., 2008; Yönlü et al., 2017), with the largest magnitude reaching *Mw* 8.2 (Carena et al., 2023). Fault that cut through the crust provide channels for material and energy to rise up from mantle, which makes EAFZ geothermal gas contain a high proportion of mantle-derived compositions (Aydin et al., 2020; Italiano et al., 2013; Yuce et al., 2014).

However, the transport of geothermal gas and geothermal water appears to be decoupled. On the one hand, deep geothermal fluid stays deep under the influence of gravity and less diffusive, compare to geothermal gas. On the other hand, the geothermal fluid was diluted due to the infiltration of a large amount of shallow cold water after the double earthquakes in February 2023 (*Mw* 7.8 *and Mw* 7.6). Our interpretation can better explain the lack of deep fluid signal in the geothermal water studied in this study. Subsequently, at a depth of 4km, gas-water interaction process was experienced. Finally rose to the surface and discharged into the atmosphere. On the contrary, the circulating geothermal water has undergone complex water-rock interaction processes such as gypsum, calcite, dolomite, anorthite and serpentinization (Fig. ~~8~~9).

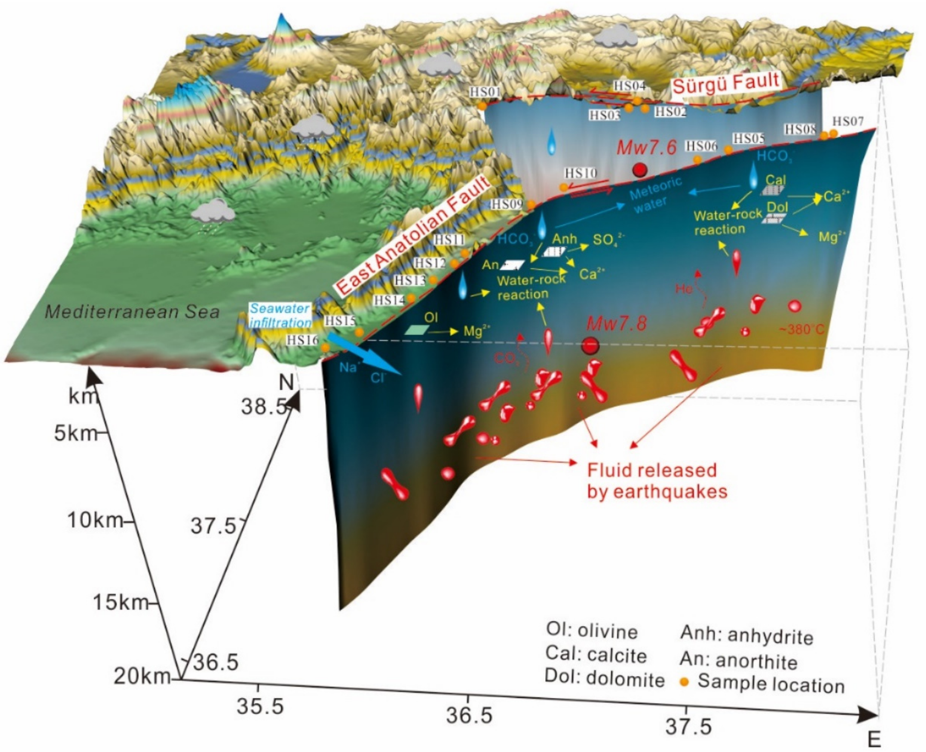


**Fig. 9. The genesis model of the geothermal fluids in the EAFZ. The deep geothermal fluid was diluted due to the infiltration of a large amount of shallow cold water. In the shallow crust, gas-water interaction process and water-rock interaction processes were experienced. The gases rose to the surface and discharged into the**

atmosphere. The circulating groundwater has undergone complex such as anhydrite, calcite, dolomite, anorthite and serpentinization.

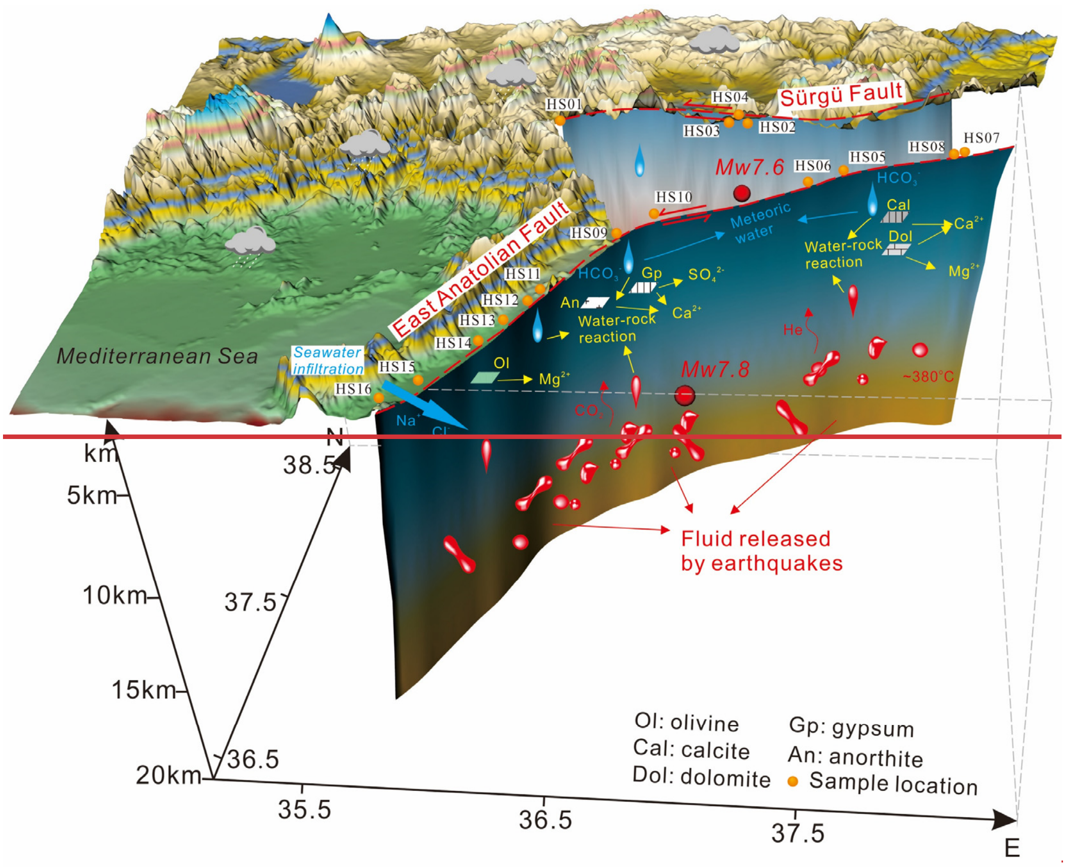


~~Figure 8. The genesis model of the geothermal fluids in the EAFZ. The deep geothermal fluid was diluted due to the infiltration of a large amount of shallow cold water. In the shallow crust, gas-water interaction process and water-rock interaction processes were experienced. The gases rose to the surface and discharged into the atmosphere. The circulating geothermal water has undergone complex such as gypsum, calcite, dolomite, anorthite and serpentinization.~~

### *5.4 The relationship between geothermal fluid and earthquake forecasting*

Earthquake forecasting is a grand goal pursued by human beings, but also one of the most difficult goals. Various physical, chemical and biological techniques are used for earthquake forecasting (Bayrak et al., 2015; Güleç et al., 2002; Kwiatek et al., 2023; Luo et al., 2024; Luo et al., 2023; Miller et al., 2004; Nalbant et al., 2002; Skelton et al., 2014; Tsunogai and Wakita, 1995; Wakita et al., 1980). As a link between the shallow (crust) and the deep (mantle), geothermal fluids can react to various diseases just like human blood. In earlier studies, researchers found that the anomaly of chemical indicators in geothermal fluids could be used for earthquake forecasting e.g., (Güleç et al., 2002; King et al., 2006; Miller et al., 2004; Perez et al., 2008; Poitrasson et al., 1999; Tsunogai and Wakita, 1995), but due to limited technology and funding, such research requiring long-term and large-scale monitoring is difficult to carry out (Ingebritsen and Manga, 2014). With the advancement of technology, more and more automated equipment and the development of 5G communication technology make long-term automatic monitoring possible, e.g., (Barbieri et al., 2021; Boschetti et al., 2022; Franchini et al., 2021; Liang et al., 2023; Luo et al., 2024; Luo et al., 2023; Skelton et al., 2014; Wang et al., 2023a). However, before geothermal fluid is really used in earthquake prediction, there is a problem that must be solved (i.e. to understand the relationship between geothermal fluid and earthquake). Its essence is to restore the origin and evolution process of geothermal fluid (Boschetti et al., 2022).

For a long time, researchers have been searching for the information of the deep fluid in the fault zone, trying to link the earthquake with the deep fluid activity (Liang et al., 2023; Luo et al., 2023; Yan et al., 2024). However, deep information is easily changed during upward migration, and sometimes even lacks deep information, just like the EAFZ geothermal water in this study (Fig. 6d). This seems to limit the ability of geothermal water to be used for earthquake prediction. In fact, chemical anomalies related to seismic activity can still be found in some shallow circulating geothermal water (e.g., $SO_4^{2-}$) (Luo et al., 2023). Moreover, the shallower water-rock interactions are more sensitive to the environment. Gypsum is widely distributed in nature, and its formation is related to evaporite. Gypsum dissolution and precipitation are often observed in geothermal water. Its solubility is greatly affected by environmental conditions (temperature, pH, pressure etc.) and is a potential indicator of earthquake prediction. After the 2023 *Mw* 7.8 and 2023 *Mw* 7.6 earthquake, in the absence of deep fluid signals, we observed anhydrite dissolution at central-southern segments of EAFZ, which are likely to have been affected by seismic activity (Fig. 6). Similar $SO_4^{2-}$ anomalies have also been found in the eastern Tibetan Plateau (Li et al., 2021; Luo et al., 2023) and southeast China (Wang et al., 2021). Therefore, we suggest that anhydrite can be used as a potential tectonic activity index.

However, although anhydrite's potential as a tectonic activity proxy is significant, its shallow crustal occurrence renders it susceptible to climatic perturbations (e.g., rainfall, evaporation). As evidenced in Fig. 6, post-seismic $SO_4^{2-}$ and $Ca^{2+}$ concentrations show no statistically significant deviations from background levels during quiescent periods, underscoring the challenge of filtering out climatic noise. While statistical correlations tentatively position anhydrite dissolution as a fault activity indicator, advancing this paradigm requires: Long-term, high-resolution monitoring to disentangle tectonic vs. meteoric signals; Mechanistic models integrating fracture permeability dynamics with anhydrite solubility kinetics.

This study's key contribution lies in establishing fault-driven permeability changes as a viable driver of anhydrite dissolution. We propose a novel conceptual framework for fault activity monitoring via groundwater systems—one that prioritizes reactive minerals in shallow water-rock interactions over traditional deep fluid signals.

After the 2023 *Mw* 7.8 and 2023 *Mw* 7.6 earthquake in EAFZ, in the absence of deep fluid signals, we observed at least three locations of gypsum dissolution, which are likely to have been affected by seismic activity (Fig. 6). Similar $SO_4^{2-}$ anomalies have also been found in the eastern Tibetan Plateau (Li et al., 2021; Luo et al., 2023) and southeast China (Wang et al., 2021). Therefore, we suggest that gypsum can be used as a potential earthquake early warning index, and the synergistic changes of $SO_4^{2-}$, $Ca^{2+}$, Sr and Ba may be used as precursor anomalies of earthquakes.

Here, we want to say that although gypsum has the potential to be used for earthquake warning, it is largely affected by climate, rainfall and environmental changes because it is located in the shallow crust. We suggest that the application of gypsum and other shallow minerals should be treated with caution, and the influence of various factors on the solubility of gypsum should be fully considered. We are urging more detailed work needs to be carried out to improve the theoretical system of the relationship between geothermal fluid and earthquake.

## 6 Conclusions

Segmented groundwater provenance: Northern groundwaters represent mixing between mantle-derived magmatic fluids (0–7%) and shallow meteoric waters, while central-southern systems are dominated by carbonate-evaporite weathering with localized seawater/halite inputs.

Tectono-Climatic controls on water-rock interactions: Plagioclase-carbonate dissolution dominates northern segments, whereas anhydrite dissolution (30–100%) in central-southern segments correlates with fault permeability changes. Seismically enhanced fracture networks amplify evaporite dissolution, driving hydrochemical anomalies.

Anhydrite as a tectonic activity tracer: Despite climatic noise, anhydrite dissolution kinetics exhibit stress-state sensitivity. Their ubiquity and rapid stress response position anhydrite as a potential tracer for real-time fault activity monitoring.

## 6 Conclusion and Outlook

We have conducted systematic element and isotope analysis on the hydrogeochemistry of geothermal fluid after the earthquake. The geothermal water temperature of EAFZ varies from 8.1°C to 32°C, and the pH changes from 7.03°C to 11.72°C. The types of geothermal water include Na-Cl-$HCO_3$, Ca-$HCO_3$, Ca-$HCO_3$-$SO_4$ and Mg-$HCO_3$. The $SiO_2$ thermometer estimates that the heat storage temperature is 19.81°C to 128.09°C, and the maximum circulation depth is 4.4km. Combined with the geological background, measured data and numerical simulation results, we propose that the geothermal resources of EAFZ is characterized by low or moderate temperature geothermal systems.

In EAFZ, the cycle process of geothermal water and geothermal gas is decoupled. Gravity and large dilution of shallow cold water may be responsible for the water-gas decoupling. The geothermal gas has obvious characteristics of volcanic sources and/or deep-rooted regional faults, while the geothermal water lacks deep fluid signal, which is mainly controlled by the shallow circulation of meteoric waters. $SO_4^{2-}$, $Ca^{2+}$, $Mg^{2+}$, Sr and Ba in geothermal water are obviously affected by water-rock interactions. The

~~water-rock interactions include the dissolution of gypsum, calcite, dolomite, anorthite and serpentinization process.~~

~~Shallow sedimentary minerals, such as gypsum, have the potential to be used as earthquake warning indicators. When earthquakes occur, the changes in the external conditions lead to changes in the solubility of gypsum, which in turn show abnormal concentrations of $SO_4^{2-}$, $Ca^{2+}$, Sr and Ba in geothermal water. However, the solubility of gypsum is controlled by many factors (e.g., temperature, pressure, climatic conditions, seasonal changes etc.), which heavily reduces the practical value of gypsum for earthquake early warning.~~

***Code and data availability.*** All water data are listed in the text or in the Supporting Information.

***Supplement.*** See Supporting Information.

***Authorship contributions.*** **Zebin Luo:** Conceptualization, Methodology, Software, Writing–Original Draft, Writing–Review and Editing. **Xiaocheng Zhou:** Conceptualization, Validation. **Yueren Xu:** Investigation. **Peng Liang:** Investigation. **Huiping Zhang:** Investigation. **Jinlong Liang:** Validation. **Zhaojun Zeng:** Investigation. **Yucong Yan:** Investigation. **Zheng Gong:** Investigation. **Shiguang Wang:** Investigation. **Chuanyou Li:** Investigation. **Zhikun Ren:** Investigation. **Jingxing Yu:** Investigation. **Zifa Ma:** Investigation. **Junjie Li:** Investigation.

***Competing Interests.*** The authors declare that they have no known competing financial interests or personal relationships that could have appeared to influence the work reported in this paper.

***Acknowledgements.*** We would like to thank the Associate Editor Prof. Heng Dai, Walter D'Alessandro Giovanni Martinelli, Hafidha Khebizi and another anonymous reviewers for their constructive comments, suggestions and corrections. We also thank Dr. Yinchun Wang Dr. Renjie Li and Dr. Yi Yu for discussion, Dr. Shiqi Zhang for her help for diagram drawing.~~and anonymous reviewers for their constructive comments, suggestions and corrections. We also thank Dr. Yinchun Wang Dr. Renjie Li and Dr. Yi Yu for discussion, Dr. Shiqi Zhang for her help for diagram drawing.~~

***Financial support.*** The work was funded by National Key Research and Development Project (2024ZD1000503，2023YFC3012005-1), Central Public-interest Scientific Institution Basal Research

Fund (CEAIEF20240405, CEAIEF2022030200, CEAIEF2022030205), the National Natural Science Foundation of China (41673106, 4193000170), IGCP Project 724.

## References


Aydin, H., Karakuş, H., and Mutlu, H.: Hydrogeochemistry of geothermal waters in eastern Turkey: Geochemical and isotopic constraints on water-rock interaction, Journal of Volcanology and Geothermal Research, 390, 2020.

Baba, A., Şaroğlu, F., Akkuş, I., Özel, N., Yeşilnacar, M. İ., Nalbantçılar, M. T., Demir, M. M., Gökçen, G., Arslan, Ş., Dursun, N., Uzelli, T., and Yazdani, H.: Geological and hydrogeochemical properties of geothermal systems in the southeastern region of Turkey, Geothermics, 78, 255-271, 2019.

Banner, J. L.: Radiogenic isotopes: systematics and applications to earth surface processes and chemical stratigraphy, Earth-Science Reviews, 65, 141-194, 2004.

Barbieri, M., Franchini, S., Barberio, M. D., Billi, A., Boschetti, T., Giansante, L., Gori, F., Jonsson, S., Petitta, M., Skelton, A., and Stockmann, G.: Changes in groundwater trace element concentrations before seismic and volcanic activities in Iceland during 2010-2018, Science of the Total Environment, 793, 2021.

Bayrak, E., Yılmaz, Ş., Softa, M., Türker, T., and Bayrak, Y.: Earthquake hazard analysis for East Anatolian Fault Zone, Turkey, Natural Hazards, 76, 1063-1077, 2015.

Bernat, M., Church, T., and Allegre, C. J.: Barium and strontium concentrations in Pacific and Mediterranean sea water profiles by direct isotope dilution mass spectrometry, Earth and Planetary Science Letters, 16, 75-80, 1972.

Bilim, F., Aydemir, A., Kosaroglu, S., and Bektas, O.: Effects of the Karacadag Volcanic Complex on the thermal structure and geothermal potential of southeast Anatolia, Bulletin of Volcanology, 80, 2018.

Boschetti, T., Barbieri, M., Barberio, M. D., Skelton, A., Stockmann, G., and Toscani, L.: Geothermometry and water-rock interaction modelling at Hafralkur: Possible implications of temperature and CO2 on hydrogeochemical changes previously linked to earthquakes in northern Iceland, Geothermics, 105, 2022.

Carena, S., Friedrich, A. M., Verdecchia, A., Kahle, B., Rieger, S., and Kübler, S.: Identification of Source Faults of Large Earthquakes in the Turkey‐Syria Border Region Between 1000 CE and the Present, and Their Relevance for the 2023 Mw 7.8 Pazarcık Earthquake, Tectonics, 42, 2023.

Craig, H.: Isotopic Variations in Meteoric Waters, Science, 133, 1702-1703, 1961.

D'Alessandro, W., Yüce, G., Italiano, F., Bellomo, S., Gülbay, A. H., Yasin, D. U., and Gagliano, A. L.: Large compositional differences in the gases released from the Kizildag ophiolitic body (Turkey): Evidences of prevailingly abiogenic origin, Marine and Petroleum Geology, 89, 174-184, 2018.

Franchini, S., Agostini, S., Barberio, M. D., Barbieri, M., Billi, A., Boschetti, T., Pennisi, M., and Petitta, M.: HydroQuakes, central Apennines, Italy: Towards a hydrogeochemical monitoring network for seismic precursors and the hydro-seismo-sensitivity of boron, Journal of Hydrology, 598, 2021.

Giggenbach, W. F.: Isotopic shifts in waters from geothermal and volcanic systems along convergent plate boundaries and their origin, Earth and Planetary Science Letters, 113, 495-510, 1992.

Güleç, N. and Hilton, D. R.: Turkish geothermal fields as natural analogues of $CO_2$

storage sites: Gas geochemistry and implications for CO 2 trapping mechanisms, Geothermics, 64, 96-110, 2016.

Güleç, N., Hilton, D. R., and Mutlu, H.: Helium isotope variations in Turkey:: relationship to tectonics, volcanism and recent seismic activities, Chemical Geology, 187, 129-142, 2002.

Güngör Yeşilova, P. and Baran, O.: Origin and Paleoenvironmental Conditions of the Köprüağzı Evaporites (Eastern Anatolia, Turkey): Sedimentological, Mineralogical and Geochemical Constraints, Minerals, 13, 282, 2023.

Hubert-Ferrari, A., Lamair, L., Hage, S., Schmidt, S., Çağatay, M. N., and Avşar, U.: A 3800 yr paleoseismic record (Lake Hazar sediments, eastern Turkey): Implications for the East Anatolian Fault seismic cycle, Earth and Planetary Science Letters, 538, 2020.

Ingebritsen, S. E. and Manga, M.: EARTHQUAKES Hydrogeochemical precursors, Nature Geoscience, 7, 697-698, 2014.

Inguaggiato, C., Censi, P., D'Alessandro, W., and Zuddas, P.: Geochemical characterisation of gases along the dead sea rift: Evidences of mantle-co2 degassing, Journal of Volcanology and Geothermal Research, 320, 50-57, 2016.

Italiano, F., Sasmaz, A., Yuce, G., and Okan, O. O.: Thermal fluids along the East Anatolian Fault Zone (EAFZ): Geochemical features and relationships with the tectonic setting, Chemical Geology, 339, 103-114, 2013.

Karaoğlu, Ö., Bazargan, M., Baba, A., and Browning, J.: Thermal fluid circulation around the Karliova triple junction: Geochemical features and volcano-tectonic implications (Eastern Turkey), Geothermics, 81, 168-184, 2019.

Karaoğlu, Ö., Browning, J., Salah, M. K., Elshaafi, A., and Gudmundsson, A.: Depths of magma chambers at three volcanic provinces in the Karlıova region of Eastern Turkey, Bulletin of Volcanology, 80, 2018.

Karaoğlu, Ö., Gülmez, F., Göçmengil, G., Lustrino, M., Di Giuseppe, P., Manetti, P., Savaşçın, M. Y., and Agostini, S.: Petrological evolution of Karlıova-Varto volcanism (Eastern Turkey): Magma genesis in a transtensional triple-junction tectonic setting, Lithos, 364-365, 2020.

King, C.-Y., Zhang, W., and Zhang, Z.: Earthquake-induced Groundwater and Gas Changes, Pure and Applied Geophysics, 163, 633-645, 2006.

Kwiatek, G., Martinez-Garzon, P., Becker, D., Dresen, G., Cotton, F., Beroza, G. C., Acarel, D., Ergintav, S., and Bohnhoff, M.: Months-long seismicity transients preceding the 2023 M(W) 7.8 Kahramanmaras earthquake, Turkiye, Nat Commun, 14, 7534, 2023.

Lanari, R., Boutoux, A., Faccenna, C., Herman, F., Willett, S. D., and Ballato, P.: Cenozoic exhumation in the Mediterranean and the Middle East, Earth-Science Reviews, 237, 2023.

Li, C., Zhou, X., Yan, Y., Ouyang, S., and Liu, F.: Hydrogeochemical Characteristics of Hot Springs and Their Short-Term Seismic Precursor Anomalies along the Xiaojiang Fault Zone, Southeast Tibet Plateau, Water, 13, 2021.

Liang, J., Yu, Y., Shi, Z., Li, Z., Huang, Y., Song, H., Xu, J., Wang, X., Zhou, X., Huang, L., Luo, Z., Tong, J., and Zhai, W.: Geothermal springs with high δ13CCO2-DIC along the Xianshuihe fault, Western Sichuan, China: A geochemical signature of enhanced deep tectonic activity, Journal of Hydrology, 623, 129760, 2023.

Liang, P., Xu, Y., Zhou, X., Li, Y., Tian, Q., Zhang, H., Ren, Z., Yu, J., Li, C., Gong, Z., Wang, S., Dou, A., Ma, Z., and Li, J.: Coseismic surface ruptures of MW7.8 and MW7.5 earthquakes occurred on February 6, 2023, and seismic hazard assessment of the East Anatolian Fault Zone, Southeastern Türkiye, Science China Earth Sciences, 68, 611-625, 2024.

Liu, X., Dong, S., Yue, Y., Guan, Q., Sun, Y., Chen, S., Zhang, J., and Yang, Y.: 87Sr/86Sr isotope ratios in rocks determined using inductively coupled plasma tandem mass spectrometry in O2 mode without prior Sr purification, Rapid Communications in Mass Spectrometry, 34, e8690, 2020.

Luo, Z., Yang, M., Zhou, X., Liu, G., Liang, J., Liu, Z., Hua, P., Ma, J., Hu, L., Sun, X., Cui, B., Wang, Z., and Chen, Y.: Evaluation of Various Forms of Geothermal Energy Release in the Beijing Region, China, Water, 16, 2024.

Luo, Z., Zhou, X., He, M., Liang, J., Li, J., Dong, J., Tian, J., Yan, Y., Li, Y., Liu, F., Ouyang, S., Liu, K., Yao, B., Wang, Y., and Zeng, Z.: Earthquakes evoked by lower crustal flow: Evidence from hot spring geochemistry in Lijiang-Xiaojinhe fault, Journal of Hydrology, 619, 129334, 2023.

Ma, Z., Li, C., Jiang, Y., Chen, Y., Yin, X., Aoki, Y., Yun, S. H., and Wei, S.: Space Geodetic Insights to the Dramatic Stress Rotation Induced by the February 2023 Turkey‐Syria Earthquake Doublet, Geophysical Research Letters, 51, 2024.

Maden, N. and Öztürk, S.: Seismic b-Values, Bouguer Gravity and Heat Flow Data Beneath Eastern Anatolia, Turkey: Tectonic Implications, Surveys in Geophysics, 36, 549-570, 2015.

Miller, S. A., Collettini, C., Chiaraluce, L., Cocco, M., Barchi, M., and Kaus, B.: Aftershocks driven by a high-pressure CO2 source at depth, Nature, 427, 724-727, 2004.

Nalbant, S. S., McCloskey, J., Steacy, S., and Barka, A. A.: Stress accumulation and increased seismic risk in eastern Turkey, Earth and Planetary Science Letters, 195, 291-298, 2002.

Okan, O. O., Kalender, L., and Cetindag, B.: Trace-element hydrogeochemistry of thermal waters of Karakocan (Elazig) and Mazgirt (Tunceli), Eastern Anatolia, Turkey, Journal of Geochemical Exploration, 194, 29-43, 2018.

Över, S., Demirci, A., and Özden, S.: Tectonic implications of the February 2023 Earthquakes (Mw7.7, 7.6 and 6.3) in south-eastern Türkiye, Tectonophysics, 866, 2023.

Oyan, V.: Petrogenesis of the Quaternary mafic alkaline volcanism along the African-Anatolian plates boundary in Turunçlu-Delihalil (Osmaniye) region in southern Turkey, Lithos, 314-315, 630-645, 2018.

Özkan, A., Solak, H. İ., Tiryakioğlu, İ., Şentürk, M. D., Aktuğ, B., Gezgin, C., Poyraz, F., Duman, H., Masson, F., Uslular, G., Yiğit, C. Ö., and Yavaşoğlu, H. H.: Characterization of the co-seismic pattern and slip distribution of the February 06, 2023, Kahramanmaraş (Turkey) earthquakes (Mw 7.7 and Mw 7.6) with a dense GNSS network, Tectonophysics, 866, 2023.

Pan, S., Kong, Y., Wang, K., Ren, Y., Pang, Z., Zhang, C., Wen, D., Zhang, L., Feng, Q., Zhu, G., and Wang, J.: Magmatic origin of geothermal fluids constrained by geochemical evidence: Implications for the heat source in the northeastern Tibetan Plateau, Journal of Hydrology, 603, 2021.

Parkhurst, D. L. and Appelo, C. A. J.: Description of input and examples for PHREEQC version 3: a computer program for speciation, batch-reaction, one-dimensional transport, and inverse geochemical calculations, U.S. Geological Survey, Reston, VA, 2013.

Pasvanoglu, S.: Geochemistry and conceptual model of thermal waters from Ercis - Zilan Valley, Eastern Turkey, Geothermics, 86, 2020.

Perez, N. M., Hernandez, P. A., Igarashi, G., Trujillo, I., Nakai, S., Sumino, H., and Wakita, H.: Searching and detecting earthquake geochemical precursors in CO2-rich groundwaters from Galicia, Spain, Geochemical Journal, 42, 75-83, 2008.

Poitrasson, F., Dundas, S. H., Toutain, J.-P., Munoz, M., and Rigo, A.: Earthquake-related elemental and isotopic lead anomaly in a springwater, Earth and Planetary Science Letters, 169, 269-276, 1999.

Pousse‐Beltran, L., Nissen, E., Bergman, E. A., Cambaz, M. D., Gaudreau, É., Karasözen, E., and Tan, F.: The 2020 Mw 6.8 Elazığ (Turkey) Earthquake Reveals Rupture Behavior of the East Anatolian Fault, Geophysical Research Letters, 47, 2020.

Sano, Y. and Wakita, H.: Geographical distribution of 3He/4He ratios in Japan: Implications for arc tectonics and incipient magmatism, Journal of Geophysical Research: Solid Earth, 90, 8729-8741, 1985.

Simão, N. M., Nalbant, S. S., Sunbul, F., and Komec Mutlu, A.: Central and eastern Anatolian crustal deformation rate and velocity fields derived from GPS and earthquake data, Earth and Planetary Science Letters, 433, 89-98, 2016.

Skelton, A., Andren, M., Kristmannsdottir, H., Stockmann, G., Morth, C.-M., Sveinbjoernsdottir, A., Jonsson, S., Sturkell, E., Gudorunardottir, H. R., Hjartarson, H., Siegmund, H., and Kockum, I.: Changes in groundwater chemistry before two consecutive earthquakes in Iceland, Nature Geoscience, 7, 752-756, 2014.

Sparacino, F., Galuzzi, B. G., Palano, M., Segou, M., and Chiarabba, C.: Seismic coupling for the Aegean - Anatolian region, Earth-Science Reviews, 228, 2022.

Tan, O., Tapirdamaz, M. C., and Yoruk, A.: The earthquake catalogues for Turkey, Turkish Journal of Earth Sciences, 17, 405-418, 2008.

Tsunogai, U. and Wakita, H.: Precursory chemical changes in ground water: kobe earthquake, Japan, Science (New York, N.Y.), 269, 61-63, 1995.

van Hinsbergen, D. J. J., Gürer, D., Koç, A., and Lom, N.: Shortening and extrusion in the East Anatolian Plateau: How was Neogene Arabia-Eurasia convergence tectonically accommodated?, Earth and Planetary Science Letters, 641, 2024.

Wakita, H., Nakamura, Y., Kita, I., Fujii, N., and Notsu, K.: Hydrogen release: new indicator of fault activity, Science (New York, N.Y.), 210, 188-190, 1980.

Wang, B., Zhou, X., Zhou, Y., Yan, Y., Li, Y., Ouyang, S., Liu, F., and Zhong, J.: Hydrogeochemistry and Precursory Anomalies in Thermal Springs of Fujian (Southeastern China) Associated with Earthquakes in the Taiwan Strait, Water, 13, 2021.

Wang, Y., Zhou, X., Tian, J., Zhou, J., He, M., Li, J., Dong, J., Yan, Y., Liu, F., Yao, B., Wang, Y., Zeng, Z., Liu, K., Li, L., Li, Z., and Xing, L.: Volatile characteristics and fluxes of He-CO2 systematics in the southeastern Tibetan Plateau: Constraints on regional seismic activities, Journal of Hydrology, 617, 2023a.

Wang, Z., Zhang, W., Taymaz, T., He, Z., Xu, T., and Zhang, Z.: Dynamic Rupture

Process of the 2023 Mw 7.8 Kahramanmaraş Earthquake (SE Türkiye): Variable Rupture Speed and Implications for Seismic Hazard, Geophysical Research Letters, 50, 2023b.

Whitney, D. L., Delph, J. R., Thomson, S. N., Beck, S. L., Brocard, G. Y., Cosca, M. A., Darin, M. H., Kaymakci, N., Meijers, M. J. M., Okay, A. I., Rojay, B., Teyssier, C., and Umhoefer, P. J.: Breaking plates: Creation of the East Anatolian fault, the Anatolian plate, and a tectonic escape system, Geology, 51, 673-677, 2023.

Yan, Y., Zhang, Z., Zhou, X., Wang, G., He, M., Tian, J., Dong, J., Li, J., Bai, Y., Zeng, Z., Wang, Y., Yao, B., Xing, G., Cui, S., and Shi, Z.: Geochemical characteristics of hot springs in active fault zones within the northern Sichuan-Yunnan block: Geochemical evidence for tectonic activity, Journal of Hydrology, 635, 2024.

YASİN, D. and YÜCE, G.: Isotope and hydrochemical characteristics of thermal waters along the active fault zone (Erzin-Hatay/Turkey) and their geothermal potential, Turkish Journal of Earth Sciences, 32, 721-739, 2023.

Yönlü, Ö., Altunel, E., and Karabacak, V.: Geological and geomorphological evidence for the southwestern extension of the East Anatolian Fault Zone, Turkey, Earth and Planetary Science Letters, 469, 1-14, 2017.

Yuce, G., Italiano, F., D'Alessandro, W., Yalcin, T. H., Yasin, D. U., Gulbay, A. H., Ozyurt, N. N., Rojay, B., Karabacak, V., Bellomo, S., Brusca, L., Yang, T., Fu, C. C., Lai, C. W., Ozacar, A., and Walia, V.: Origin and interactions of fluids circulating over the Amik Basin (Hatay, Turkey) and relationships with the hydrologic, geologic and tectonic settings, Chemical Geology, 388, 23-39, 2014.

Yuce, G. and Taskiran, L.: Isotope and chemical compositions of thermal fluids at Tekman Geothermal Area (Eastern Turkey), GEOCHEMICAL JOURNAL, 47, 423-435, 2013.

Zeng, Z., Yang, L., Cui, Y., Zhou, X., He, M., Wang, Y., Yan, Y., Yao, B., Hu, X., Shao, W., Li, J., and Fu, H.: Assessment of geothermal waters in Yunnan, China: Distribution, quality and driving factors, Geothermics, 130, 103323, 2025.

Zhou, Z., Thybo, H., Artemieva, I. M., Kusky, T., and Tang, C.-C.: Crustal melting and continent uplift by mafic underplating at convergent boundaries, Nature Communications, 15, 2024.

Aydin, H., Karakuş, H., and Mutlu, H.: Hydrogeochemistry of geothermal waters in eastern Turkey: Geochemical and isotopic constraints on water-rock interaction, Journal of Volcanology and Geothermal Research, 390, 2020.

Baba, A., Şaroğlu, F., Akkuş, I., Özel, N., Yeşilnacar, M. İ., Nalbantçılar, M. T., Demir, M. M., Gökçen, G., Arslan, Ş., Dursun, N., Uzelli, T., and Yazdani, H.: Geological and hydrogeochemical properties of geothermal systems in the southeastern region of Turkey, Geothermics, 78, 255-271, 2019.

Barbieri, M., Franchini, S., Barberio, M. D., Billi, A., Boschetti, T., Giansante, L., Gori, F., Jonsson, S., Petitta, M., Skelton, A., and Stockmann, G.: Changes in groundwater trace element concentrations before seismic and volcanic activities in Iceland during 2010-2018, Science of the Total Environment, 793, 2021.

Bayrak, E., Yılmaz, Ş., Softa, M., Türker, T., and Bayrak, Y.: Earthquake hazard analysis for East Anatolian Fault Zone, Turkey, Natural Hazards, 76, 1063-1077, 2015.

Bilim, F., Aydemir, A., Kosaroglu, S., and Bektas, O.: Effects of the Karacadag Volcanic Complex on the thermal structure and geothermal potential of southeast Anatolia, Bulletin of Volcanology, 80, 2018.

Boschetti, T., Barbieri, M., Barberio, M. D., Skelton, A., Stockmann, G., and Toscani, L.: Geothermometry and water-rock interaction modelling at Hafralkur: Possible implications of temperature and CO2 on hydrogeochemical changes previously linked to earthquakes in northern Iceland, Geothermics, 105, 2022.

Carena, S., Friedrich, A. M., Verdecchia, A., Kahle, B., Rieger, S., and Kübler, S.: Identification of Source Faults of Large Earthquakes in the Turkey - Syria Border Region Between 1000 CE and the Present, and Their Relevance for the 2023 Mw 7.8 Pazarcık Earthquake, Tectonics, 42, 2023.

Cipolli, F., Gambardella, B., Marini, L., Ottonello, G., and Zuccolini, M. V.: Geochemistry of high-pH waters from serpentinites of the Gruppo di Voltri (Genova, Italy) and reaction path modeling of CO<sub>2</sub> sequestration in serpentinite aquifers, Applied Geochemistry, 19, 787-802, 2004.

Craig, H.: Isotopic Variations in Meteoric Waters, Science, 133, 1702-1703, 1961.

Fournier, R. O.: Chemical geothermometers and mixing models for geothermal systems, Geothermics, 5, 41-50, 1977.

Franchini, S., Agostini, S., Barberio, M. D., Barbieri, M., Billi, A., Boschetti, T., Pennisi, M., and Petitta, M.: HydroQuakes, central Apennines, Italy: Towards a hydrogeochemical monitoring network for seismic precursors and the hydro-seismo-sensitivity of boron, Journal of Hydrology, 598, 2021.

Güleç, N. and Hilton, D. R.: Turkish geothermal fields as natural analogues of CO 2 storage sites: Gas geochemistry and implications for CO 2 trapping mechanisms, Geothermics, 64, 96-110, 2016.

Güleç, N., Hilton, D. R., and Mutlu, H.: Helium isotope variations in Turkey:: relationship to tectonics, volcanism and recent seismic activities, Chemical Geology, 187, 129-142, 2002.

Hem, J. D.: Study and interpretation of the chemical characteristics of natural water, Geological Survey water-supply paper (USA), 2254, 1985.

Huang;, R., Shang;, X., Zhao;, Y., Sun;, W., and Liu;, X.: Effect of Fluid Salinity on Reaction Rate and Molecular Hydrogen ($H_2$) Formation During Peridotite Serpentinization at 300°C, Journal of Geophysical Research Solid Earth, 128, e2022JB025218, 2023.

Hubert-Ferrari, A., Lamair, L., Hage, S., Schmidt, S., Çağatay, M. N., and Avşar, U.: A 3800 yr paleoseismic record (Lake Hazar sediments, eastern Turkey): Implications for the East Anatolian Fault seismic cycle, Earth and Planetary Science Letters, 538, 2020.

Ingebritsen, S. E. and Manga, M.: EARTHQUAKES Hydrogeochemical precursors, Nature Geoscience, 7, 697-698, 2014.

Inguaggiato, C., Censi, P., D'Alessandro, W., and Zuddas, P.: Geochemical characterisation of gases along the dead sea rift: Evidences of mantle-co2 degassing, Journal of Volcanology and Geothermal Research, 320, 50-57, 2016.

Italiano, F., Sasmaz, A., Yuce, G., and Okan, O. O.: Thermal fluids along the East Anatolian Fault Zone (EAFZ): Geochemical features and relationships with the tectonic

setting, Chemical Geology, 339, 103-114, 2013.
Karaoğlu, Ö., Bazargan, M., Baba, A., and Browning, J.: Thermal fluid circulation around the Karliova triple junction: Geochemical features and volcano-tectonic implications (Eastern Turkey), Geothermics, 81, 168-184, 2019.
Karaoğlu, Ö., Browning, J., Salah, M. K., Elshaafi, A., and Gudmundsson, A.: Depths of magma chambers at three volcanic provinces in the Karlıova region of Eastern Turkey, Bulletin of Volcanology, 80, 2018.
Karaoğlu, Ö., Gülmez, F., Göçmengil, G., Lustrino, M., Di Giuseppe, P., Manetti, P., Savaşçın, M. Y., and Agostini, S.: Petrological evolution of Karlıova-Varto volcanism (Eastern Turkey): Magma genesis in a transtensional triple-junction tectonic setting, Lithos, 364-365, 2020.
King, C.-Y., Zhang, W., and Zhang, Z.: Earthquake-induced Groundwater and Gas Changes, Pure and Applied Geophysics, 163, 633-645, 2006.
Kretzschmar, H. J. and Wagner, W.: International Steam Tables Properties of Water and Steam based on the Industrial Formulation IAPWS-IF97, Springer Vieweg Berlin, Heidelberg, 2019.
Kwiatek, G., Martinez-Garzon, P., Becker, D., Dresen, G., Cotton, F., Beroza, G. C., Acarel, D., Ergintav, S., and Bohnhoff, M.: Months-long seismicity transients preceding the 2023 M(W) 7.8 Kahramanmaras earthquake, Turkiye, Nat Commun, 14, 7534, 2023.
Lanari, R., Boutoux, A., Faccenna, C., Herman, F., Willett, S. D., and Ballato, P.: Cenozoic exhumation in the Mediterranean and the Middle East, Earth Science Reviews, 237, 2023.
Li, C., Zhou, X., Yan, Y., Ouyang, S., and Liu, F.: Hydrogeochemical Characteristics of Hot Springs and Their Short-Term Seismic Precursor Anomalies along the Xiaojiang Fault Zone, Southeast Tibet Plateau, Water, 13, 2021.
Liang, J., Yu, Y., Shi, Z., Li, Z., Huang, Y., Song, H., Xu, J., Wang, X., Zhou, X., Huang, L., Luo, Z., Tong, J., and Zhai, W.: Geothermal springs with high δ13CCO2-DIC along the Xianshuihe fault, Western Sichuan, China: A geochemical signature of enhanced deep tectonic activity, Journal of Hydrology, 623, 129760, 2023.
Luo, Z., Yang, M., Zhou, X., Liu, G., Liang, J., Liu, Z., Hua, P., Ma, J., Hu, L., Sun, X., Cui, B., Wang, Z., and Chen, Y.: Evaluation of Various Forms of Geothermal Energy Release in the Beijing Region, China, Water, 16, 2024.
Luo, Z., Zhou, X., He, M., Liang, J., Li, J., Dong, J., Tian, J., Yan, Y., Li, Y., Liu, F., Ouyang, S., Liu, K., Yao, B., Wang, Y., and Zeng, Z.: Earthquakes evoked by lower crustal flow: Evidence from hot spring geochemistry in Lijiang-Xiaojinhe fault, Journal of Hydrology, 619, 129334, 2023.
Ma, Z., Li, C., Jiang, Y., Chen, Y., Yin, X., Aoki, Y., Yun, S. H., and Wei, S.: Space Geodetic Insights to the Dramatic Stress Rotation Induced by the February 2023 Turkey - Syria Earthquake Doublet, Geophysical Research Letters, 51, 2024.
Maden, N. and Öztürk, S.: Seismic b-Values, Bouguer Gravity and Heat Flow Data Beneath Eastern Anatolia, Turkey: Tectonic Implications, Surveys in Geophysics, 36, 549-570, 2015.
Miller, S. A., Collettini, C., Chiaraluce, L., Cocco, M., Barchi, M., and Kaus, B.: Aftershocks driven by a high-pressure CO2 source at depth, Nature, 427, 724-727, 2004.

Nalbant, S. S., McCloskey, J., Steacy, S., and Barka, A. A.: Stress accumulation and increased seismic risk in eastern Turkey, Earth and Planetary Science Letters, 195, 291-298, 2002.

Ni, S., Sun, H., Somerville, P., Yuen, D. A., Milliner, C., Wang, H., Zhou, J., and Cui, Y.: Complexities of the Turkey-Syria doublet earthquake sequence, Innovation, 4, 2023.

Över, S., Demirci, A., and Özden, S.: Tectonic implications of the February 2023 Earthquakes (Mw7.7, 7.6 and 6.3) in south-eastern Türkiye, Tectonophysics, 866, 2023.

Özkan, A., Solak, H. İ., Tiryakioğlu, İ., Şentürk, M. D., Aktuğ, B., Gezgin, C., Poyraz, F., Duman, H., Masson, F., Uslular, G., Yiğit, C. Ö., and Yavaşoğlu, H. H.: Characterization of the co-seismic pattern and slip distribution of the February 06, 2023, Kahramanmaraş (Turkey) earthquakes (Mw 7.7 and Mw 7.6) with a dense GNSS network, Tectonophysics, 866, 2023.

Pan, S., Kong, Y., Wang, K., Ren, Y., Pang, Z., Zhang, C., Wen, D., Zhang, L., Feng, Q., Zhu, G., and Wang, J.: Magmatic origin of geothermal fluids constrained by geochemical evidence: Implications for the heat source in the northeastern Tibetan Plateau, Journal of Hydrology, 603, 2021.

Parkhurst, D. L. and Appelo, C. A. J.: Description of input and examples for PHREEQC version 3: a computer program for speciation, batch-reaction, one-dimensional transport, and inverse geochemical calculations, U.S. Geological Survey, Reston, VA, 2013.

Perez, N. M., Hernandez, P. A., Igarashi, G., Trujillo, I., Nakai, S., Sumino, H., and Wakita, H.: Searching and detecting earthquake geochemical precursors in CO2-rich groundwaters from Galicia, Spain, Geochemical Journal, 42, 75-83, 2008.

Poitrasson, F., Dundas, S. H., Toutain, J.-P., Munoz, M., and Rigo, A.: Earthquake-related elemental and isotopic lead anomaly in a springwater, Earth and Planetary Science Letters, 169, 269-276, 1999.

Pousse‐Beltran, L., Nissen, E., Bergman, E. A., Cambaz, M. D., Gaudreau, É., Karasözen, E., and Tan, F.: The 2020 Mw 6.8 Elazığ (Turkey) Earthquake Reveals Rupture Behavior of the East Anatolian Fault, Geophysical Research Letters, 47, 2020.

Simão, N. M., Nalbant, S. S., Sunbul, F., and Komec Mutlu, A.: Central and eastern Anatolian crustal deformation rate and velocity fields derived from GPS and earthquake data, Earth and Planetary Science Letters, 433, 89-98, 2016.

Skelton, A., Andren, M., Kristmannsdottir, H., Stockmann, G., Morth, C.-M., Sveinbjoernsdottir, A., Jonsson, S., Sturkell, E., Gudorunardottir, H. R., Hjartarson, H., Siegmund, H., and Kockum, I.: Changes in groundwater chemistry before two consecutive earthquakes in Iceland, Nature Geoscience, 7, 752-756, 2014.

Sparacino, F., Galuzzi, B. G., Palano, M., Segou, M., and Chiarabba, C.: Seismic coupling for the Aegean - Anatolian region, Earth-Science Reviews, 228, 2022.

Tan, O., Tapirdamaz, M. C., and Yoruk, A.: The earthquake catalogues for Turkey, Turkish Journal of Earth Sciences, 17, 405-418, 2008.

Tsunogai, U. and Wakita, H.: Precursory chemical changes in ground water: kobe earthquake, Japan, Science (New York, N.Y.), 269, 61-63, 1995.

van Hinsbergen, D. J. J., Gürer, D., Koç, A., and Lom, N.: Shortening and extrusion in the East Anatolian Plateau: How was Neogene Arabia-Eurasia convergence tectonically accommodated?, Earth and Planetary Science Letters, 641, 2024.

Wakita, H., Nakamura, Y., Kita, I., Fujii, N., and Notsu, K.: Hydrogen release: new indicator of fault activity, Science (New York, N.Y.), 210, 188-190, 1980.

Wang, B., Zhou, X., Zhou, Y., Yan, Y., Li, Y., Ouyang, S., Liu, F., and Zhong, J.: Hydrogeochemistry and Precursory Anomalies in Thermal Springs of Fujian (Southeastern China) Associated with Earthquakes in the Taiwan Strait, Water, 13, 2021.

Wang, Y., Zhou, X., Tian, J., Zhou, J., He, M., Li, J., Dong, J., Yan, Y., Liu, F., Yao, B., Wang, Y., Zeng, Z., Liu, K., Li, L., Li, Z., and Xing, L.: Volatile characteristics and fluxes of He-CO2 systematics in the southeastern Tibetan Plateau: Constraints on regional seismic activities, Journal of Hydrology, 617, 2023a.

Wang, Z., Zhang, W., Taymaz, T., He, Z., Xu, T., and Zhang, Z.: Dynamic Rupture Process of the 2023 Mw 7.8 Kahramanmaraş Earthquake (SE Türkiye): Variable Rupture Speed and Implications for Seismic Hazard, Geophysical Research Letters, 50, 2023b.

Wei, Z.-A., Shao, H., Tang, L., Deng, B., Li, H., and Wang, C.: Hydrogeochemistry and geothermometry of geothermal waters from the Pearl River Delta region, South China, Geothermics, 96, 2021.

Whitney, D. L., Delph, J. R., Thomson, S. N., Beck, S. L., Brocard, G. Y., Cosca, M. A., Darin, M. H., Kaymakci, N., Meijers, M. J. M., Okay, A. I., Rojay, B., Teyssier, C., and Umhoefer, P. J.: Breaking plates: Creation of the East Anatolian fault, the Anatolian plate, and a tectonic escape system, Geology, 51, 673-677, 2023.

Yan, Y., Zhang, Z., Zhou, X., Wang, G., He, M., Tian, J., Dong, J., Li, J., Bai, Y., Zeng, Z., Wang, Y., Yao, B., Xing, G., Cui, S., and Shi, Z.: Geochemical characteristics of hot springs in active fault zones within the northern Sichuan-Yunnan block: Geochemical evidence for tectonic activity, Journal of Hydrology, 635, 2024.

Yönlü, Ö., Altunel, E., and Karabacak, V.: Geological and geomorphological evidence for the southwestern extension of the East Anatolian Fault Zone, Turkey, Earth and Planetary Science Letters, 469, 1-14, 2017.

Yuce, G., Italiano, F., D'Alessandro, W., Yalcin, T. H., Yasin, D. U., Gulbay, A. H., Ozyurt, N. N., Rojay, B., Karabacak, V., Bellomo, S., Brusca, L., Yang, T., Fu, C. C., Lai, C. W., Ozacar, A., and Walia, V.: Origin and interactions of fluids circulating over the Amik Basin (Hatay, Turkey) and relationships with the hydrologic, geologic and tectonic settings, Chemical Geology, 388, 23-39, 2014.

Zhou, Z., Thybo, H., Artemieva, I. M., Kusky, T., and Tang, C.-C.: Crustal melting and continent uplift by mafic underplating at convergent boundaries, Nature Communications, 15, 2024.